



2  
2006

**LIBRARY  
Michigan State  
University**

This is to certify that the  
dissertation entitled

**INVERSE MEDIUM SCATTERING FOR  
ELECTROMAGNETIC WAVE PROPAGATION**

presented by

Peijun Li

has been accepted towards fulfillment  
of the requirements for the

Ph.D. degree in Applied Mathematics



Major Professor's Signature

07/28/05

Date

**PLACE IN RETURN BOX** to remove this checkout from your record.  
**TO AVOID FINES** return on or before date due.  
**MAY BE RECALLED** with earlier due date if requested.

DATE DUE	DATE DUE	DATE DUE
080609		
		AUG 30 2008

**INVERSE MEDIUM SCATTERING FOR  
ELECTROMAGNETIC WAVE PROPAGATION**

**By**

**Peijun Li**

**A DISSERTATION**

**Submitted to  
Michigan State University  
in partial fulfillment of the requirements  
for the degree of**

**DOCTOR OF PHILOSOPHY**

**Department of Mathematics**

**2005**

## ABSTRACT

### INVERSE MEDIUM SCATTERING FOR ELECTROMAGNETIC WAVE PROPAGATION

By

Peijun Li

This thesis focuses on the study of continuation methods for solving inverse medium scattering problems from electromagnetic wave propagation.

The first part considers a time-harmonic electromagnetic plane wave incident on a medium enclosed by a bounded domain in  $\mathbb{R}^3$ . A continuation method for the inverse medium scattering problem, which reconstructs the scatterer of an inhomogeneous medium from boundary measurements of the scattered wave, is developed. The algorithm requires multi-frequency scattering data. Using an initial guess from the Born approximation, each update is obtained via recursive linearization on the wavenumber  $k$  by solving one forward problem and one adjoint problem of Maxwell's equations.

In part two, we consider the inverse medium scattering problem for Helmholtz's equation at fixed frequency. A new continuation method for the inverse medium scattering is developed. The algorithm requires only single-frequency scattering data. Using an initial guess from the Born approximation, each update is obtained via recursive linearization on the spatial frequency of a one-parameter family of plane waves by solving one forward and one adjoint problem of the Helmholtz equation.

To my son, Ray.

## ACKNOWLEDGMENTS

With great pleasure, I would like to express my sincere gratitude to all those who assisted and helped me while I was studying and doing research for this dissertation.

First and foremost I am deeply grateful to Prof. Gang Bao, my thesis advisor, for his guidance and assistance, for his encouragement and support, and for his kindness and hospitality during my graduate study at Michigan State University. I would like to thank him for suggesting problems and giving directions which sheds light not only on my current research but also on my future career.

I wish to express special thanks to Prof. Tien-Yien Li, who shows me some mathematical insights and gives me his support without reservation. I would like to thank Prof. Zhengfang Zhou for his inspiring discussions and suggestions. Also I would like to thank Prof. Chichia Chiu, Prof. Guowei Wei, and Prof. Keith Promislow for their time and concern.

I am forever indebted to my wife, Ying Zhang, and my family for their enduring patience, constant support, and encouragement.

# TABLE OF CONTENTS

<b>LIST OF FIGURES</b>	<b>vi</b>
<b>LIST OF TABLES</b>	<b>ix</b>
<b>Introduction</b>	<b>1</b>
<b>1 Inverse Medium Scattering Problems for Electromagnetic Waves</b>	<b>4</b>
1.1 Introduction . . . . .	4
1.2 Analysis of the Variational Problem for Forward Scattering . . . . .	7
1.3 Inverse Medium Scattering . . . . .	14
1.3.1 Low-Frequency Modes of the Scatterer . . . . .	15
1.3.2 Recursive Linearization . . . . .	18
1.4 Numerical Experiments . . . . .	25
1.5 Concluding Remarks . . . . .	35
<b>2 Inverse Medium Scattering at Fixed Frequency</b>	<b>42</b>
2.1 Introduction . . . . .	42
2.2 Analysis of the Scattering Map . . . . .	48
2.3 Inverse Medium Scattering . . . . .	57
2.3.1 Born Approximation . . . . .	58
2.3.2 Recursive Linearization . . . . .	60
2.4 Numerical Experiments . . . . .	66
2.5 Concluding Remarks . . . . .	87
<b>BIBLIOGRAPHY</b>	<b>88</b>

## LIST OF FIGURES

1.1	Parsity pattern of an FE matrix with 1820 unknowns: (a) original ordering; (b) RCM ordering. . . . .	27
1.2	Example 1: Integrals at different wavenumbers for the fixed incident angle $\theta = \pi/3$ and $\phi = \pi/3$ . Solid curve: the exact integral value of the left-hand side of (1.3.2), +: the computed integral value of the first term of the right-hand side of (1.3.2), *: the computed integral value of the second term of right-hand side of (1.3.2), o: the computed integral value of the right-hand side of (1.3.2). . . . .	29
1.3	Example 1: Integrals with different $\theta$ for the fixed wave number $k = 2.0$ and $\phi = \pi/3$ . Solid curve: the exact integral value of the left-hand side of (1.3.2), o: the computed integral value of the right hand-side of (1.3.2). . . . .	30
1.4	Example 1: Integrals with different $\phi$ for the fixed wave number $k = 2.0$ and $\theta = \pi/3$ . Solid curve: the exact integral value of the left-hand side of (1.3.2), o: the computed integral value of the right-hand side of (1.3.2). . . . .	31
1.5	Example 1: (a) the slice $x = 0$ of the true scatterer; (b) the slice $x = 0$ of the reconstruction. . . . .	32
1.6	Example 1: (a) the slice $y = 0$ of the true scatterer; (b) the slice $y = 0$ of the reconstruction. . . . .	33
1.7	Example 1: (a) the slice $z = 0$ of the true scatterer; (b) the slice $z = 0$ of the reconstruction. . . . .	34
1.8	Example 2: Integrals at different wavenumbers for the fixed incident angle $\theta = \pi/3$ and $\phi = \pi/3$ . Solid curve: the exact integral value of the left-hand side of (1.3.2), +: the computed integral value of the first term of the right-hand side of (1.3.2), *: the computed integral value of the second term of right-hand side of (1.3.2), o: the computed integral value of the right-hand side of (1.3.2). . . . .	36
1.9	Example 2: Integrals with different $\theta$ for the fixed wave number $k = 3.0$ and $\phi = \pi/3$ . Solid curve: the exact integral value of the left-hand side of (1.3.2), o: the computed integral value of the right hand-side of (1.3.2). . . . .	37

1.10	Example 2: Integrals with different $\phi$ for the fixed wave number $k = 2.0$ and $\theta = \pi/3$ . Solid curve: the exact integral value of the left-hand side of (1.3.2), $\circ$ : the computed integral value of the right-hand side of (1.3.2).	38
1.11	Example 2: (a) the slice $x = 0$ of the true scatterer; (b) the slice $x = 0$ of the reconstruction.	39
1.12	Example 2: (a) the slice $y = -0.5$ of the true scatterer; (b) the slice $y = -0.5$ of the reconstruction.	40
1.13	Example 2: (a) the slice $z = 0$ of the true scatterer; (b) the slice $z = 0$ of the reconstruction.	41
2.1	Evanescent plane wave at $k_0 = 4.0$ with $\eta = 4.7$ .	44
2.2	Evanescent plane wave at $k_0 = 4.0$ with $\eta = 8.0$ .	45
2.3	Example 1: true scatterer $q_1$ .	68
2.4	Example 1: Born approximation.	69
2.5	Example 1: reconstruction of $q_1$ at $\eta = 10.2$ .	70
2.6	Example 1: reconstruction of $q_1$ at $\eta = 8.4$ .	71
2.7	Example 1: reconstruction of $q_1$ at $\eta = 6.6$ .	72
2.8	Example 1: reconstruction of $q_1$ at $\eta = 4.8$ .	73
2.9	Example 1: reconstruction of $q_1$ at $\eta = 3.0$ .	74
2.10	Example 1: reconstruction of $q_1$ at $\eta = 0.0$ .	75
2.11	Example 1. Relative error of the reconstruction $q_1$ at different wavenumber $k_0$ . $\circ$ : reconstruction at $k_0 = 10.0$ ; $*$ : reconstruction at $k_0 = 8.0$ ; $\square$ : reconstruction at $k_0 = 6.0$ ; $+$ : reconstruction at $k_0 = 4.0$ .	76
2.12	Example 1. Relative error of the reconstruction $q_1$ at different step size $\delta\eta$ . $\circ$ : reconstruction at $\delta\eta = 0.6$ ; $*$ : reconstruction at $\delta\eta = 1.2$ ; $\square$ : reconstruction at $\delta\eta = 2.0$ .	77
2.13	Example 2: true scatterer of $q_2$ .	79
2.14	Example 2: reconstruction of $q_2$ .	80
2.15	Example 2: contour view of the true scatterer $q_2$ .	81
2.16	Example 2: contour view of the reconstructed scatterer $q_2$ .	81
2.17	Example 2. Evolution of slice for the reconstruction $q_2$ . Solid line: true scatterer; Circle: reconstruction. Top row from left to right: reconstruction at $\eta = 14.45$ ; reconstruction at $\eta = 13.60$ ; reconstruction at $\eta = 12.75$ ; middle row from left to right: reconstruction at $\eta = 10.20$ ; reconstruction at $\eta = 8.50$ ; reconstruction at $\eta = 6.80$ ; bottom row from left to right: reconstruction at $\eta = 5.10$ ; reconstruction at $\eta = 2.55$ ; reconstruction at $\eta = 0.0$ .	82

2.18 Example 3: true scatterer of $q_3$ . . . . .	83
2.19 Example 3: reconstructed scatterer of $q_3$ . . . . .	84
2.20 Example 3: image view of the true scatterer $q_3$ . . . . .	85
2.21 Example 3: image view of the reconstructed scatterer $q_3$ . . . . .	86

## LIST OF TABLES

1.1	Recursive linearization reconstruction algorithm for inverse medium scattering. . . . .	24
1.2	Relative error at different wavenumbers of Example 1. . . . .	28
1.3	Relative error at different wavenumbers of Example 2. . . . .	35
2.1	Recursive linearization reconstruction algorithm. . . . .	65

# Introduction

Consider an electromagnetic plane wave propagating in a homogeneous medium. In the absence of any inhomogeneities, the wave will continue to propagate and nothing of physical interest will happen. However, if there are inhomogeneities present, the wave will be scattered and we can express the total field as the sum of original incident wave and the scattered wave. The behavior of the scattered wave will depend on both the incident wave and the nature of the inhomogeneities in the medium. The direct problem, given this information, is to find the scattered wave. The inverse problem takes this answer to the direct scattering problem as its starting point and ask, what is the nature of the inhomogeneities that gave rise to such scattered field behavior?

This thesis focuses on the study of continuation methods for solving inverse scattering problems. These inverse scattering problems arise naturally from diverse applications such as medical imaging, nondestructive testing, and geophysical exploration [10]. Two major difficulties for solving these inverse problems by optimization methods are the ill-posedness and the presence of many local minima. Based on multi-experimental data with physical parameters, we have developed regularized continuation methods to solve the inverse medium scattering for three-dimensional time-harmonic Maxwell's equations and the inverse medium scattering for Helmholtz equation at fixed frequency.

In Chapter 1, we consider a time-harmonic electromagnetic plane wave incident on a medium enclosed by a bounded domain in  $\mathbb{R}^3$ . Existence and uniqueness of the

variational problem for direct scattering are established. An energy estimate for the scattered field with a uniform bound with respect to the wavenumber is obtained in the case of low frequency on which the Born approximation is based.

The inverse medium scattering problem is to determine the scatterer from the measurements of near field currents densities on the boundary, given the incident field. Although this is a classical problem in inverse scattering theory, little is known on reconstruction methods, especially in the three dimensional case, due to the non-linearity, ill-posedness, and the large scale computation associated with the inverse scattering problem. Our goal is to present a recursive linearization method that solves the inverse medium scattering problem of Maxwell's equations in three dimensions. The algorithm requires multi-frequency scattering data, and the recursive linearization is obtained by a continuation method on the wavenumber  $k$ . It first solves a linear equation (Born approximation) at the lowest  $k$ , which may be done by using the Fast Fourier Transform. Updates are subsequently obtained by using higher and higher wavenumber  $k$ . Using the idea of Kaczmarz method, we use partial data to perform the nonlinear Landweber iteration at each stage of the wavenumber  $k$ . For each iteration, one forward and one adjoint state of the Maxwell's equations are solved. This may be implemented by using the symmetric second order edge (Nédélec) elements.

Chapter 2 considers a time-harmonic electromagnetic plane wave incident on a medium enclosed by a bounded domain in  $\mathbb{R}^2$ . Existence and uniqueness of the variational problem for the direct scattering are established. An energy estimate for the scattered field is obtained on which the Born approximation is based. Fréchet differentiability of the scattering map is examined.

The main purpose of this work is to present a single-frequency inversion method, and to demonstrate the efficiency of a new continuation method for the inverse medium scattering. The illuminating fields, including the high spatial frequency evanescent plane waves, form a one-parameter family of plane waves. When the ob-

ject is probed with the high spatial frequency of the evanescent plane waves, only a thin layer of the object is penetrated. Corresponding to this exponentially decaying incident field, the scattered field which is measured on the boundary contains information of the object in that thin layer. Such a measurement is entirely inadequate to determine the whole object. However, the measurement may be used to obtain an approximation. The evanescent plane waves with less spatial frequency are needed to illuminate the object. While the probing energy penetrates a thicker layer of the object, the relation between the measurement and the scatterer to be recovered in the thicker layer becomes more nonlinear. These nonlinear equations can be considered as perturbations to the already solved equations at the previous thicker layers, and therefore can be continually and recursively linearized with standard perturbational techniques. Thus, the recursive linearization is a continuation method on the transverse direction of the incident waves, which controls the depth of its penetration.

# CHAPTER 1

## Inverse Medium Scattering Problems for Electromagnetic Waves

### 1.1 Introduction

Consider the systems of time harmonic Maxwell's equations in three dimensions

$$\nabla \times E^t = i\omega\mu^*H^t, \quad (1.1.1)$$

$$\nabla \times H^t = -i\omega\varepsilon^*E^t, \quad (1.1.2)$$

where  $E^t$  and  $H^t$  are the total electric field and magnetic field, respectively;  $\omega > 0$  is the frequency; and  $\varepsilon^*$  and  $\mu^*$  are the electric permittivity and the magnetic permeability, respectively. Denote by  $\varepsilon_0 > 0$ ,  $\mu_0 > 0$  the permittivity and permeability of the vacuum. The fields are further assumed to be nonmagnetic; i.e.  $\mu^* = \mu_0$ . Rewriting  $\varepsilon^* = \varepsilon_0\varepsilon$ ,  $\varepsilon = 1 + q(x)$  is the relative permittivity, where  $q(x)$  is the scatterer, which is assumed to have a compact support, and  $\Re(q(x)) > -1$ .

Taking the curl of (1.1.1) and eliminating the magnetic field  $H^t$ , we obtain the

uncoupled equation for the electric field  $E^t$ :

$$\nabla \times (\nabla \times E^t) - k^2 \varepsilon E^t = 0, \quad (1.1.3)$$

where  $k = \omega \sqrt{\varepsilon_0 \mu_0}$  is called the wavenumber, satisfying  $0 < k_{\min} \leq k \leq k_{\max} < \infty$ .

The total electric field  $E^t$  consists of the incident field  $E^i$  and the scattered field  $E$ :

$$E^t = E^i + E.$$

Assume that the incident field is a plane wave of the normalized form [10]

$$E^i = ik\vec{p}e^{ikx \cdot \vec{n}}, \quad (1.1.4)$$

where  $\vec{n} \in \mathbb{S}^2$  is the propagation direction and  $\vec{p} \in \mathbb{S}^2$  is the polarization satisfying  $\vec{p} \cdot \vec{n} = 0$ . Evidently, such an incident wave satisfies the homogeneous equation

$$\nabla \times (\nabla \times E^i) - k^2 E^i = 0. \quad (1.1.5)$$

It follows from the equations (1.1.3) and (1.1.5) that the scattered field satisfies

$$\nabla \times (\nabla \times E) - k^2 \varepsilon E = k^2 q(x) E^i. \quad (1.1.6)$$

In addition, the scattered field is required to satisfy the following Silver–Müller radiation condition:

$$\lim_{r \rightarrow \infty} r[\nabla \times E \times \frac{x}{r} - ikE] = 0,$$

where  $r = |x|$ . In practice, it is convenient to reduce the problem to a bounded domain by introducing an artificial surface. Let  $\Omega$  be the compact support of the scatterer  $q(x)$ . Assume that  $R > 0$  is a constant, such that the support of the scatterer,  $\Omega$ ,

is included in the ball  $B = \{x \in \mathbb{R}^3 : |x| < R\}$ . Let  $S$  be the sphere of the ball, i.e.  $S = \{x \in \mathbb{R}^3 : |x| = R\}$ . Denote  $\nu$  the outward unit normal to  $S$ . A suitable boundary condition then has to be imposed on  $S$ . For simplicity, we employ the first order absorbing boundary condition (impedance boundary condition) [22] as

$$\nu \times (\nabla \times E) + ik\nu \times (\nu \times E) = 0 \quad \text{on } S. \quad (1.1.7)$$

Given the incident field  $E^i$ , the forward problem is to determine the scattered field  $E$  for the known scatterer  $q(x)$ , which is assumed further to be in  $L^\infty(B)$ . Based on the Helmholtz decomposition and a compact imbedding result, the forward problem is shown to have a unique solution for all but possibly a discrete set of wavenumbers. Furthermore, an energy estimate for the scattered field, with a uniform bound with respect to the wavenumber, is given in the low frequency case. The estimate provides a theoretical basis for our linearization algorithm. For numerical solution of the forward scattering problem in an open domain, the reader is referred to [25, 26, 27, 32] and references therein. The inverse medium scattering problem is to determine the scatterer  $q(x)$  from the measurements of near field current densities, the tangential trace of the scattered field  $\nu \times E|_S$ , given the incident field. Although this is a classical problem in inverse scattering theory, little is known on reconstruction methods, especially in the three dimensional case, due to the nonlinearity, ill-posedness, and large scale computation associated with the inverse scattering problem. We refer the reader to [1, 13, 19, 20, 34] for related results on the inverse medium problem. See [10] for an account of recent progress on the general inverse scattering problem.

The goal of this work is to present a recursive linearization method that solves the inverse medium scattering problem of Maxwell's equations in three dimensions. The reader is referred to [3, 8] for recursive linearization approaches for solving the inverse medium scattering problems in two dimensions. Our algorithm requires multi-

frequency scattering data, and the recursive linearization is obtained by a continuation method on the wavenumber. It first solves a linear equation (Born approximation) at the lowest wavenumber, which may be done by using the fast Fourier transform (FFT). Updates are subsequently obtained by using higher and higher wavenumbers. Following the idea of the Kaczmarz method [29, 30, 13], we use partial data to perform the nonlinear Landweber iteration at each wavenumber. For each iteration, one forward and one adjoint state of Maxwell's equations are solved, which may be implemented by using the symmetric second order edge (Nédélec) elements.

The plan of this paper is as follows. Analysis of the variational problem for forward scattering is presented in section 1.2. Based on the Helmholtz decomposition, a compact imbedding result, and the Lax–Milgram lemma, the well-posedness of the forward scattering is proved. An important energy estimate is given. Section 1.3 is devoted to the numerical study of inverse medium scattering. Using the initial guess of the reconstruction derived from the Born approximation, a regularized iterative linearization algorithm is proposed. Numerical examples are presented in section 1.4. The paper is concluded with some remarks and future directions in section 1.5.

## 1.2 Analysis of the Variational Problem for Forward Scattering

In this section, the variational formulation for the forward scattering problem is discussed. The analysis provides a criterion for weak scattering, which plays an important role in the inversion algorithm.

To state our boundary value problem, following [28], we first introduce the stan-

standard Sobolev spaces:

$$L_t^2(S) = \{u \in (L^2(S))^3 : \nu \cdot u = 0 \text{ on } S\},$$

$$H_0^1(B) = \{u \in H^1(B) : u = 0 \text{ on } S\},$$

$$H(\text{curl}, B) = \{u \in (L^2(B))^3 : \nabla \times u \in (L^2(B))^3\},$$

$$H_{\text{imp}}(\text{curl}, B) = \{u \in H(\text{curl}, B) : \nu \times u \in L_t^2(S)\},$$

where  $H_{\text{imp}}(\text{curl}, B)$  is an appropriate subspace of  $H(\text{curl}, B)$  for solving problems involving the impedance boundary condition. Correspondingly, these spaces are equipped with the norms

$$\|u\|_{L_t^2(S)} = \|u\|_{(L^2(S))^3},$$

$$\|u\|_{H^1(B)}^2 = \|u\|_{L^2(B)}^2 + \|\nabla u\|_{(L^2(B))^3}^2,$$

$$\|u\|_{H(\text{curl}, B)}^2 = \|u\|_{(L^2(B))^3}^2 + \|\nabla \times u\|_{(L^2(B))^3}^2,$$

$$\|u\|_{H_{\text{imp}}(\text{curl}, B)}^2 = \|u\|_{H(\text{curl}, B)}^2 + \|\nu \times u\|_{L_t^2(S)}^2.$$

For convenience, denote the  $(L^2(B))^3$  and  $(L^2(S))^3$  inner products by

$$(u, v) = \int_B u \cdot \bar{v} dx \quad \text{and} \quad \langle u, v \rangle = \int_S u \cdot \bar{v} ds,$$

respectively, where the overline denotes the complex conjugate. Introduce the bilinear form  $a : H_{\text{imp}}(\text{curl}, B) \times H_{\text{imp}}(\text{curl}, B) \rightarrow \mathbb{C}$ ;

$$a(E, \phi) = (\nabla \times E, \nabla \times \phi) - k^2(\varepsilon E, \phi) + ik\langle \nu \times E, \nu \times \phi \rangle,$$

and the linear functional on  $H_{\text{imp}}(\text{curl}, B)$ ;

$$b(\phi) = k^2(qE^i, \phi).$$

Then we have the weak form of the boundary value problem (1.1.6) and (1.1.7): find  $E \in H_{\text{imp}}(\text{curl}, B)$  such that

$$a(E, \phi) = b(\phi) \quad \forall \phi \in H_{\text{imp}}(\text{curl}, B). \quad (1.2.1)$$

Throughout the paper,  $C$  stands for a positive generic constant whose value may change step by step but should always be clear from the context.

Before presenting the main result for the variational problem, we state several useful lemmas. The reader is referred to [28] for detailed discussions and proofs.

**Lemma 1.2.1 (Helmholtz decomposition).** *The spaces  $X$  and  $Y$  are closed subspaces of  $H_{\text{imp}}(\text{curl}, B)$ , which is the direct sum of the spaces  $X$  and  $Y$ , i.e.,*

$$H_{\text{imp}}(\text{curl}, B) = X \oplus Y.$$

Here

$$X = \{u \in H_{\text{imp}}(\text{curl}, B) : \text{div}(\varepsilon u) = 0, \text{ in } B\}$$

and

$$Y = \{\nabla \xi : \xi \in H_0^1(B)\}.$$

**Lemma 1.2.2 (compact imbedding).** *The space  $X$  is compactly imbedded into the space  $(L^2(B))^3$ .*

**Lemma 1.2.3 (Friedrichs inequality).** *There exists a positive constant  $C$ , inde-*

pendent of the wavenumber, such that for all  $u \in X$

$$\| u \|_{(L^2(B))^3} \leq C \left( \| \nabla \times u \|_{(L^2(B))^3} + \| \nu \times u \|_{(L^2(S))^3} \right).$$

Next we prove the well-posedness of the variational problem (1.2.1) and obtain an energy estimate for the scattered field with a uniform bound with respect to the wavenumber in the case of low frequency.

**Theorem 1.2.1.** *If the wavenumber is sufficiently small, the variational problem (1.2.1) admits a unique weak solution in  $H_{\text{imp}(\text{curl}, B)}$  given by  $E = u + \nabla p$ , while  $u \in X, p \in H_0^1(B)$ . Furthermore, we have the estimate*

$$\| E \|_{H_{\text{imp}(\text{curl}, B)}} \leq C k |\Omega|^{1/2} \| q \|_{L^\infty(B)}, \quad (1.2.2)$$

where the constant  $C$  is independent of  $k$  and  $\Omega$  is the compact support of the scatterer.

**PROOF.** Using the Helmholtz decomposition, we take  $E = u + \nabla p$  and  $\phi = v + \nabla \xi$ , for any  $v \in X, \xi \in H_0^1(B)$ . Observe that  $a(u, \nabla \xi) = 0$ , for any  $\xi \in H_0^1(B)$ , by the definition of  $X$ . Therefore, we decompose the variational equation (1.2.1) into the form

$$a(u, v) + a(\nabla p, v) + a(\nabla p, \nabla \xi) = b(v) + b(\nabla \xi) \quad \forall v \in X, \xi \in H_0^1(B). \quad (1.2.3)$$

First, we determine  $p \in H_0^1(B)$  by the solution of

$$a(\nabla p, \nabla \xi) = b(\nabla \xi) \quad \forall \xi \in H_0^1(B),$$

which gives explicitly

$$-(\varepsilon \nabla p, \nabla \xi) = (q E^i, \nabla \xi) \quad \forall \xi \in H_0^1(B).$$

The existence and uniqueness of the solution  $p$  in  $H_0^1(B)$  may be proved by a direct application of the Lax–Milgram lemma with the estimate

$$\| \nabla p \|_{(L^2(B))^3} \leq Ck|\Omega|^{1/2} \| q \|_{L^\infty(B)}. \quad (1.2.4)$$

Rewrite (1.2.3) as

$$a(u, v) = b(v) - a(\nabla p, v) \quad \forall v \in X \quad (1.2.5)$$

and decompose the bilinear form  $a$  into  $a = a_1 + k^2 a_2$ , where

$$\begin{aligned} a_1(u, v) &= (\nabla \times u, \nabla \times v) + ik \langle \nu \times u, \nu \times v \rangle, \\ a_2(u, v) &= -(\varepsilon u, v). \end{aligned}$$

Using the inequality of arithmetic and geometric means, we conclude from Lemma 1.2.3 that  $a_1$  is coercive

$$|a_1(u, u)| \geq Ck \left( \| \nabla \times u \|_{(L^2(B))^3}^2 + \| \nu \times u \|_{(L^2(S))^3}^2 \right) \geq Ck \| u \|_{H_{\text{imp}}(\text{curl}, B)}^2 \quad \forall u \in X.$$

The continuity of the bilinear form  $a_1$  follows from the Cauchy–Schwarz inequality.

Next we prove the compactness of  $a_2$ . Define an operator  $\mathcal{A} : (L^2(B))^3 \rightarrow X$  by

$$a_1(\mathcal{A}u, v) = a_2(u, v) \quad \forall v \in X,$$

which gives

$$(\nabla \times \mathcal{A}u, \nabla \times v) + ik \langle \nu \times \mathcal{A}u, \nu \times v \rangle = -(\varepsilon u, v) \quad \forall v \in X.$$

Using the Lax–Milgram lemma again, it follows that

$$\| \mathcal{A}u \|_{H_{\text{imp}}(\text{curl}, B)} \leq \frac{C}{k} \| u \|_{(L^2(B))^3}, \quad (1.2.6)$$

where the constant  $C$  is independence of  $k$ . Thus  $\mathcal{A}$  is bounded from  $(L^2(B))^3$  to  $X$ , and  $X$  is compactly imbedded into  $(L^2(B))^3$ . Hence  $\mathcal{A} : (L^2(B))^3 \rightarrow (L^2(B))^3$  is a compact operator.

Define a function  $w \in (L^2(B))^3$  by requiring  $w \in X$  and satisfying

$$a_1(w, v) = b(v) - a(\nabla p, v) \quad \forall v \in X.$$

More specifically, we have by using the Stokes formula that

$$a_1(w, v) = k^2(qE^i, v) + k^2(\varepsilon \nabla p, v) \quad \forall v \in X.$$

It follows from the Lax-Milgram Lemma that

$$\| w \|_{H_{\text{imp}}(\text{curl}, B)} \leq C \left( k^2 |\Omega|^{1/2} \| q \|_{L^\infty(B)} + k \| \nabla p \|_{(L^2(B))^3} \right).$$

An application of (1.2.4) yields

$$\| w \|_{H_{\text{imp}}(\text{curl}, B)} \leq C k^2 |\Omega|^{1/2} \| q \|_{L^\infty(B)}. \quad (1.2.7)$$

Using the operator  $\mathcal{A}$ , we can see that the problem (1.2.5) is equivalent to finding  $u \in (L^2(B))^3$  such that

$$(\mathcal{I} + k^2 \mathcal{A})u = w. \quad (1.2.8)$$

When the wavenumber  $k$  is small enough, the operator  $\mathcal{I} + k^2 \mathcal{A}$  has a uniformly

bounded inverse. We then have the estimate

$$\| u \|_{(L^2(B))^3} \leq C \| w \|_{(L^2(B))^3}, \quad (1.2.9)$$

where the constant  $C$  is independent of  $k$ . However, rearranging (1.2.8), we have  $u = w - k^2 \mathcal{A}u$ , so  $u \in X$  and, by the estimate (1.2.6) for the operator  $\mathcal{A}$ , we have

$$\| u \|_{H_{\text{imp}}(\text{curl}, B)} \leq \| w \|_{H_{\text{imp}}(\text{curl}, B)} + Ck \| u \|_{(L^2(B))^3}.$$

Combining the estimates (1.2.9) and (1.2.7) leads to

$$\| u \|_{H_{\text{imp}}(\text{curl}, B)} \leq Ck^2 |\Omega|^{1/2} \| q \|_{L^\infty(B)}. \quad (1.2.10)$$

Finally, it follows from the definition of the norm in  $H_{\text{imp}}(\text{curl}, B)$  that

$$\| E \|_{H_{\text{imp}}(\text{curl}, B)} \leq \| u \|_{H_{\text{imp}}(\text{curl}, B)} + \| \nabla p \|_{(L^2(B))^3}.$$

The proof is complete by noting the estimates (1.2.10) and (1.2.4) for sufficiently small wavenumbers.  $\square$

**Remark 1.2.1.** *The energy estimate of the scattered field (1.2.2) provides a criterion for weak scattering. From this estimate, it is easily seen that fixing any two of the three quantities, i.e. the wavenumber, the compact support of the scatterer  $\Omega$ , and the  $L^\infty(B)$  norm of the scatterer, the scattering is weak when the third one is small. Especially for the given scatterer  $q(x)$ , i.e. the norm and the compact support are fixed, the scattering is weak when the wavenumber is small.*

**Remark 1.2.2.** *For a general wavenumber, from (1.2.8), the uniqueness and existence follow from the Fredholm alternative. If the scatterer  $q(x)$  is more regular, say of  $C_0^2(B)$  [15], unique continuation may be used to prove the uniqueness and thus the*

existence of the forward scattering problem (1.1.6), (1.1.7) for all  $k > 0$ . Otherwise, if  $k^2$  is not the eigenvalue for Maxwell's equations in the domain  $B$ , then the operator  $\mathcal{I} + k^2\mathcal{A}$  has a bounded inverse. However, the bound depends on the wavenumber. Therefore, the constant  $C$  in the estimate (1.2.2) depends on the wavenumber.

From the above discussion, we have the following theorem on the well-posedness of the variational problem (1.2.1).

**Theorem 1.2.2.** *Given the scatterer  $q \in L^\infty(B)$ , for all but possibly a discrete set of wavenumbers, the variational problem (1.2.1) admits a unique weak solution in  $H_{\text{imp}}(\text{curl}, B)$ , given by  $E = u + \nabla p$ , while  $u \in X$ ,  $p \in H_0^1(B)$ .*

### 1.3 Inverse Medium Scattering

In this section, a regularized recursive linearization method for solving the inverse medium scattering problem of Maxwell's equations in three dimensions is proposed. The algorithm, obtained by a continuation method on the wavenumber, requires multifrequency scattering data. At each wavenumber, the algorithm determines a forward model which produces the prescribed scattering data. At a low wavenumber, the scattered field is weak. Consequently, the nonlinear equation becomes essentially linear, known as the Born approximation. The algorithm first solves this nearly linear equation at the lowest wavenumber to obtain low-frequency modes of the true scatterer. The approximation is then used to linearize the nonlinear equation at the next higher wavenumber to produce a better approximation which contains more modes of the true scatterer. This process is continued until a sufficiently high wavenumber, where the dominant modes of the scatterer are essentially recovered.

### 1.3.1 Low-Frequency Modes of the Scatterer

Rewrite (1.1.6) as

$$\nabla \times (\nabla \times E) - k^2 E = k^2 q(x)(E^i + E), \quad (1.3.1)$$

where the incident wave is taken as  $E^i = ik\vec{p}_1 e^{ikx \cdot \vec{n}_1}$ . Consider a test function  $F = ik\vec{p}_2 e^{ikx \cdot \vec{n}_2}$ , where  $\vec{p}_2, \vec{n}_2 \in \mathbb{S}^2$  satisfy  $\vec{p}_2 \cdot \vec{n}_2 = 0$ . Hence  $F$  satisfies (1.1.5).

Multiplying (1.3.1) by  $F$  and integrating over  $B$  on both sides, we have

$$\int_B F \cdot [\nabla \times (\nabla \times E)] dx - k^2 \int_B F \cdot E dx = k^2 \int_B q(x) F \cdot E^i dx + k^2 \int_B q(x) F \cdot E dx.$$

Integration by parts yields

$$\begin{aligned} \int_B E \cdot [\nabla \times (\nabla \times F)] dx + \int_S [E \times (\nabla \times F) - F \times (\nabla \times E)] \cdot \nu ds - k^2 \int_B F \cdot E dx \\ = k^2 \int_B q(x) F \cdot E^i dx + k^2 \int_B q(x) F \cdot E dx. \end{aligned}$$

We have, by noting (1.1.5),

$$\int_S [E \times (\nabla \times F) - F \times (\nabla \times E)] \cdot \nu ds = k^2 \int_B q(x) F \cdot E^i dx + k^2 \int_B q(x) F \cdot E dx.$$

Using the boundary condition (1.1.7) of the scattered field and the special form of the incident wave  $E^i$  and  $F$ , we get

$$\begin{aligned} - \int_S (\nu \times E) \cdot (\vec{n}_2 \times \vec{p}_2) e^{ikx \cdot \vec{n}_2} ds + \int_S [\nu \times (\nu \times E)] \cdot \vec{p}_2 e^{ikx \cdot \vec{n}_2} ds \\ = \int_B q(x) F \cdot E^i dx + \int_B q(x) F \cdot E dx. \end{aligned}$$

A simple calculation yields

$$\begin{aligned} \int_B q(x) e^{ikx \cdot (\vec{n}_1 + \vec{n}_2)} dx &= \frac{1}{(\vec{p}_1 \cdot \vec{p}_2) k^2} \int_S (\nu \times E) \cdot (\vec{n}_2 \times \vec{p}_2 + \nu \times \vec{p}_2) e^{ikx \cdot \vec{n}_2} ds \\ &\quad + \frac{i}{(\vec{p}_1 \cdot \vec{p}_2) k} \int_B q(x) \vec{p}_2 \cdot E e^{ikx \cdot \vec{n}_2} dx. \end{aligned} \quad (1.3.2)$$

From Theorem 1.2.1 and Remark 1.2.1, for a small wavenumber, the scattered field is weak and the inverse scattering problem becomes essentially linear. Dropping the nonlinear (second) term of (1.3.2), we obtain the linearized integral equation

$$\int_B q_0(x) e^{ikx \cdot (\vec{n}_1 + \vec{n}_2)} dx = \frac{1}{(\vec{p}_1 \cdot \vec{p}_2) k^2} \int_S (\nu \times E) \cdot (\vec{n}_2 \times \vec{p}_2 + \nu \times \vec{p}_2) e^{ikx \cdot \vec{n}_2} ds, \quad (1.3.3)$$

which is the Born approximation. The function  $q_0(x)$  will be used as the starting point for our recursive linearization algorithm.

Since the scatterer  $q_0(x)$  has a compact support, we use the notation

$$\hat{q}_0(\xi) = \int_B q_0(x) e^{ikx \cdot (\vec{n}_1 + \vec{n}_2)} dx,$$

where  $\hat{q}_0(\xi)$  is the Fourier transform of  $q_0(x)$  with  $\xi = k(\vec{n}_1 + \vec{n}_2)$ . Choose

$$\vec{n}_j = (\sin \theta_j \cos \phi_j, \sin \theta_j \sin \phi_j, \cos \theta_j), \quad j = 1, 2,$$

where  $\theta_j, \phi_j$  are the latitudinal and longitudinal angles, respectively. It is obvious that the domain  $[0, \pi] \times [0, 2\pi]$  of  $(\theta_j, \phi_j), j = 1, 2$ , corresponds to the ball  $\{\xi \in \mathbb{R}^3 : |\xi| \leq 2k\}$ . Thus, the Fourier modes of  $\hat{q}_0(\xi)$  in the ball  $\{\xi : |\xi| \leq 2k\}$  can be determined. The scattering data with the higher wavenumber must be used in order to recover more modes of the true scatterer.

Define the data

$$G(\zeta) = \begin{cases} \frac{1}{(\vec{p}_1 \cdot \vec{p}_2)k^2} \int_S (\nu \times E) \cdot (\vec{n}_2 \times \vec{p}_2 + \nu \times \vec{p}_2) e^{ikx \cdot \vec{n}_2} ds & \text{for } |\zeta| \leq 2k, \\ 0, & \text{otherwise,} \end{cases}$$

where  $\zeta = \zeta(k, \theta_1, \phi_1, \theta_2, \phi_2) \in \mathbb{R}^3$ . The linear integral equation (1.3.3) can then be formally reformulated as

$$\int_{\mathbb{R}^3} q_0(x) e^{ix \cdot \zeta} dx = G(\zeta). \quad (1.3.4)$$

Taking the inverse Fourier transform of (1.3.4) leads to

$$\frac{1}{(2\pi)^3} \int_{\mathbb{R}^3} e^{-ix \cdot \zeta} \left[ \int_{\mathbb{R}^3} q_0(y) e^{iy \cdot \zeta} dy \right] d\zeta = \frac{1}{(2\pi)^3} \int_{\mathbb{R}^3} e^{-ix \cdot \zeta} G(\zeta) d\zeta.$$

By the Fubini theorem, we have

$$\frac{1}{(2\pi)^3} \int_{\mathbb{R}^3} q_0(y) \left[ \int_{\mathbb{R}^3} e^{i(y-x) \cdot \zeta} d\zeta \right] dy = \frac{1}{(2\pi)^3} \int_{\mathbb{R}^3} e^{-ix \cdot \zeta} G(\zeta) d\zeta.$$

Using the inverse Fourier transform of the Dirac delta function

$$\frac{1}{(2\pi)^3} \int_{\mathbb{R}^3} e^{i(y-x) \cdot \zeta} d\zeta = \delta(y-x),$$

we deduce

$$\int_{\mathbb{R}^3} q_0(y) \delta(y-x) dy = \frac{1}{(2\pi)^3} \int_{\mathbb{R}^3} e^{-ix \cdot \xi} G(\xi) d\xi,$$

which gives

$$q_0(x) = \frac{1}{(2\pi)^3} \int_{\mathbb{R}^3} e^{-ix \cdot \zeta} G(\zeta) d\zeta. \quad (1.3.5)$$

In practice, the integral equation (1.3.5) is implemented by using the FFT.

### 1.3.2 Recursive Linearization

As discussed in the previous section, when the wavenumber is small, the Born approximation allows a reconstruction of those Fourier modes less than or equal to  $2k$  for the function  $q(x)$ . We now describe a procedure that recursively determines  $q_k$  at  $k = k_j$  for  $j = 1, 2, \dots$  with the increasing wavenumbers. Suppose now that the scatterer  $q_{\tilde{k}}$  has been recovered at some wavenumber  $\tilde{k}$ , and that the wavenumber  $k$  is slightly larger than  $\tilde{k}$ . We wish to determine  $q_k$ , or equivalently, to determine the perturbation

$$\delta q = q_k - q_{\tilde{k}}.$$

For the reconstructed scatterer  $q_{\tilde{k}}$ , we solve at the wavenumber  $k$  the forward scattering problem

$$\nabla \times (\nabla \times \tilde{E}) - k^2(1 + q_{\tilde{k}})\tilde{E} = k^2 q_{\tilde{k}} E^i, \quad x \in B, \quad (1.3.6)$$

$$\nu \times (\nabla \times \tilde{E}) + ik\nu \times (\nu \times \tilde{E}) = 0 \quad \text{on } S. \quad (1.3.7)$$

For the scatterer  $q_k$ , we have

$$\nabla \times (\nabla \times E) - k^2(1 + q_k)E = k^2 q_k E^i, \quad x \in B, \quad (1.3.8)$$

$$\nu \times (\nabla \times E) + ik\nu \times (\nu \times E) = 0 \quad \text{on } S. \quad (1.3.9)$$

Subtracting (1.3.6), (1.3.7) from (1.3.8), (1.3.9), and omitting the second order smallness in  $\delta q$  and in  $\delta E = E - \tilde{E}$ , we obtain

$$\nabla \times (\nabla \times \delta E) - k^2(1 + q_{\tilde{k}})\delta E = k^2 \delta q (E^i + \tilde{E}), \quad x \in B, \quad (1.3.10)$$

$$\nu \times (\nabla \times \delta E) + ik\nu \times (\nu \times \delta E) = 0 \quad \text{on } S. \quad (1.3.11)$$

For the scatterer  $q_k$  and the incident wave  $E^i$ , we define the map  $S(q_k, E^i)$  by

$$S(q_k, E^i) = E,$$

where  $E$  is the scattered field at the wavenumber  $k$ . Let  $\gamma$  be the trace operator to the boundary  $S$  of the ball  $B$ . Define the scattering map

$$M(q_k, E^i) = \gamma S(q_k, E^i).$$

It is easily seen that the scattering map  $M(q_k, E^i)$  is linear with respect to  $E^i$  but is nonlinear with respect to  $q_k$ . For simplicity, denote  $M(q_k, E^i)$  by  $M(q_k)$ . By the definition of the trace operator, we have

$$M(q_k) = \nu \times E|_S.$$

We refer to [1] for the Fréchet differentiability of the scattering map. Let  $DM(q_{\bar{k}})$  be the Fréchet derivative of  $M(q_{\bar{k}})$ , and denote the residual operator

$$R(q_{\bar{k}}) = \nu \times \delta E|_S.$$

It follows from [1] that

$$DM(q_{\bar{k}})\delta q = R(q_{\bar{k}}). \tag{1.3.12}$$

The regularized least-squares solution of (1.3.12) is

$$\delta q = [\alpha I + DM^*(q_{\bar{k}})DM(q_{\bar{k}})]^{-1} DM^*(q_{\bar{k}})R(q_{\bar{k}}),$$

where  $DM^*(q_{\bar{k}})$  is the adjoint operator of  $DM(q_{\bar{k}})$ ,  $I$  is the identity operator, and  $\alpha$  is some suitable positive number. In practice, the main difficulty is the enormous

computational cost of solving linear systems with huge full matrix. Here, we consider an alternative way of solving (1.3.12) which is much less computationally demanding.

To state the approach, we first examine the boundary data  $\nu \times E(x; \theta, \phi; k)$ . Here, the variable  $x$  is the observation point, which has two degrees of freedom since it is on the sphere  $S$ . The terms  $\theta, \phi$  are latitudinal and longitudinal angles respectively of the incident wave  $E^i$ . At each frequency, we have four degrees of freedom, and thus data redundancy, which may be addressed by fixing one of the incident angles, say  $\theta$ . Define  $\phi_j = (j - 1) * 2\pi/m, j = 1, \dots, m$ , and the residual operator

$$R_j(q_{\bar{k}}) = \nu \times E(x; \theta, \phi_j; k)|_S - \nu \times \tilde{E}(x; \theta, \phi_j; k)|_S,$$

where  $m$  is the total number of the incident waves or sweeps, and  $\tilde{E}(x; \theta, \phi_j; k)$  is the solution of (1.3.6), (1.3.7) with the incident wave of longitudinal angle  $\phi_j$  and the scatterer  $q_{\bar{k}}$ . Instead of solving (1.3.12) for all incident waves simultaneously, we may solve it for one incident wave at a time while updating the residual operator after each determination of the incremental correction  $\delta q$ . Thus, for each incident wave with incident angle  $\phi_j$ , we consider the equation

$$M_j(q_k) = \nu \times E(x; \theta, \phi_j; k)|_S, \tag{1.3.13}$$

where  $M_j(q_k)$  is the scattering map corresponding to the incident wave with longitudinal angle  $\phi_j$ . It follows from [1] that

$$DM_j(q_{\bar{k}})\delta q_j = R_j(q_{\bar{k}}), \tag{1.3.14}$$

where  $DM_j(q_{\bar{k}})$  is the Fréchet derivative of the scattering map  $M_j(q_k)$ . The nonlinear

Landweber iteration for (1.3.13) yields

$$\delta q_j = \beta_k DM_j^*(q_{\bar{k}}) R_j(q_{\bar{k}}), \quad (1.3.15)$$

where  $DM_j^*(q_{\bar{k}})$  is the adjoint operator of  $DM_j(q_{\bar{k}})$ , and  $\beta_k$  is some relaxation parameter [14].

**Remark 1.3.1.** *For a fixed wavenumber, the stopping index of nonlinear Landweber iteration (1.3.15) could be determined from the discrepancy principle. However, in practice, it is not necessary to do many iterations. Our numerical results indicate that the iterative process for different incident angles  $\phi_j, j = 1, \dots, m$ , is sufficient to obtain reasonable accuracy.*

Next, we discuss the role of the relaxation parameter  $\beta_k$  in the iteration (1.3.15), which may be understood more clearly by considering the iteration from a different point of view.

Consider the optimization problem of (1.3.13),

$$\min_{q_k} \| M_j(q_k) - \nu \times E(x; \theta, \phi_j; k) \|_{(L^2(S))^3}^2. \quad (1.3.16)$$

The first order optimality condition for the problem (1.3.16) is given by

$$DM_j^*(q_{\bar{k}}) (M_j(q_k) - \nu \times E(x; \theta, \phi_j; k)) |_S = 0. \quad (1.3.17)$$

To solve the optimality equation (1.3.17), the time marching scheme proposed in [33] consists of finding the steady state of the following parabolic equation:

$$\frac{dq_k}{dt} = DM_j^*(q_{\bar{k}}) (\nu \times E(x; \theta, \phi_j; k) - M_j(q_k)) |_S.$$

The numerical solution could be computed from the explicit method

$$\delta q_j = \tau DM_j^*(q_{\bar{k}})R_j(q_{\bar{k}}),$$

where  $\tau$  is the discretized time step. Thus, the relaxation parameter  $\beta_k$  is essentially the step size of time marching, whose length is restricted by the stability of the explicit method.

In order to compute the correction  $\delta q_j$ , we need some efficient way to compute  $DM_j^*(q_{\bar{k}})R_j(q_{\bar{k}})$ , which is given by the following theorem.

**Theorem 1.3.1.** *Given the residual  $R_j(q_{\bar{k}})$ , there exists a function  $F_j$  satisfying the adjoint equations*

$$\nabla \times (\nabla \times F_j) - k^2(1 + \overline{q_{\bar{k}}})F_j = 0, \quad x \in B, \quad (1.3.18)$$

$$\nabla \times F_j - ik\nu \times F_j = R_j(q_{\bar{k}}) \quad \text{on } S, \quad (1.3.19)$$

such that the adjoint Fréchet derivative  $DM_j^*(q_{\bar{k}})$  satisfies

$$[DM_j^*(q_{\bar{k}})R_j(q_{\bar{k}})](x) = k^2(\overline{E_j^i}(x) + \overline{\tilde{E}_j}(x)) \cdot F_j(x), \quad (1.3.20)$$

where  $E_j^i$  is the incident wave with the longitudinal angle  $\phi_j$  and  $\tilde{E}_j$  is the solution of (1.3.6), (1.3.7) with the incident wave  $E_j^i$ .

**PROOF.** Let  $\tilde{E}_j$  be the solution of (1.3.6), (1.3.7) with the incident wave  $E_j^i$ . Consider the equations as follows:

$$\nabla \times (\nabla \times \delta E) - k^2(1 + q_{\bar{k}})\delta E = k^2\delta q(E_j^i + \tilde{E}_j), \quad x \in B, \quad (1.3.21)$$

$$\nu \times (\nabla \times \delta E) + ik\nu \times (\nu \times \delta E) = 0 \quad \text{on } S, \quad (1.3.22)$$

and the adjoint equations (1.3.18) and (1.3.19), which take the variational form:

$$\begin{aligned} (\nabla \times F_j, \nabla \times \phi) - k^2((1 + \overline{q_{\bar{k}}})F_j, \phi) - ik\langle \nu \times F_j, \nu \times \phi \rangle \\ = \langle R_j(q_{\bar{k}}^-), \nu \times \phi \rangle, \quad \forall \phi \in H_{\text{imp}}(\text{curl}, B). \end{aligned}$$

The existence and uniqueness of the weak solution for the adjoint equations may be proved in the same way as for the scattered field. The proof is omitted.

Multiplying equation (1.3.21) with the complex conjugate of  $F_j$  integrating over  $B$  on both sides, we obtain

$$\int_B \overline{F_j} \cdot [\nabla \times (\nabla \times \delta E)] dx - k^2 \int_B (1 + q_{\bar{k}}^-) \overline{F_j} \cdot \delta E dx = k^2 \int_B \delta q (E_j^i + \tilde{E}_j) \cdot \overline{F_j} dx.$$

Integration by parts yields

$$\int_S [\delta E \times (\overline{\nabla \times F_j}) - \overline{F_j} \times (\nabla \times \delta E)] \cdot \nu ds = k^2 \int_B \delta q (E_j^i + \tilde{E}_j) \cdot \overline{F_j} dx.$$

Using the boundary condition (1.3.22), we deduce

$$\int_S (\nu \times \delta E) \cdot (\overline{\nabla \times F_j + ik\nu \times F_j}) ds = k^2 \int_B \delta q (E_j^i + \tilde{E}_j) \cdot \overline{F_j} dx.$$

It follows from (1.3.14) and the boundary condition (1.3.19) that

$$\int_S [DM_j(q_{\bar{k}}^-) \delta q] \cdot \overline{R_j(q_{\bar{k}}^-)} ds = k^2 \int_B \delta q (E_j^i + \tilde{E}_j) \cdot \overline{F_j} dx.$$

We know from the adjoint operator  $DM_j^*(q_{\bar{k}}^-)$  that

$$\int_B \delta q \overline{DM_j^*(q_{\bar{k}}^-) R_j(q_{\bar{k}}^-)} dx = k^2 \int_B \delta q (E_j^i + \tilde{E}_j) \cdot \overline{F_j} dx.$$

---

Initialization:

$k = k_{\min}$     smallest  $k_{\min}$

$q_0$     Born approximation

Reconstruction loop:

FOR  $k = k_{\min} : k_{\max}$     march along wavenumbers

  FOR  $j = 1 : m$     perform  $m$  sweeps over incident angles

    solve (1.3.6)-(1.3.7) for  $\tilde{E}_j$     one forward problem

    solve (1.3.18)-(1.3.19) for  $F_j$     one adjoint problem

$\delta q_k^j = \beta_k k^2 (\overline{E_j^i} + \overline{\tilde{E}_j}) \cdot F_j$

$q_k^j := q_k^j + \delta q_k^j$

  END

$q_k := q_k^m$

END

$q := q_{k_{\max}}$     final reconstruction

---

Table 1.1. Recursive linearization reconstruction algorithm for inverse medium scattering.

Since this holds for any  $\delta q$ , we have

$$\overline{DM_j^*(q_{\tilde{k}})R_j(q_{\tilde{k}})} = k^2(E_j^i + \tilde{E}_j) \cdot \bar{F}_j.$$

Taking the complex conjugate of the above equation yields the result.  $\square$

Using this theorem, we can rewrite (1.3.15) as

$$\delta q_j = \beta_k k^2 (\overline{E_j^i}(x) + \overline{\tilde{E}_j}(x)) \cdot F_j(x). \quad (1.3.23)$$

Thus, for each incident wave with a longitudinal angle  $\phi_j$ , we solve one forward problem (1.3.6), (1.3.7) and one adjoint problem (1.3.18), (1.3.19). Since the adjoint problem has a variational form similar as the forward problem, we need to compute essentially two forward problems at each sweep. Once  $\delta q_j$  is determined,  $q_{\tilde{k}}$  is updated by  $q_{\tilde{k}} + \delta q_j$ . After completing the  $m$ th sweep, we get the reconstructed scatterer  $q_k$

at the wavenumber  $k$ .

The recursive linearization for inverse medium scattering of Maxwell's equations can be summarized in Table 1.1.

## 1.4 Numerical Experiments

In this section, we discuss the numerical solution of the forward scattering problem and the computational issues of the recursive linearization algorithm.

As for the forward solver, we adopt the edge elements which were developed originally for the finite element solution of Maxwell's equations [31, 22] in the beginning of the 1980s. From the mathematical point of view, these are natural approximation spaces for the Hilbert space  $H(\text{curl}, B)$ , which is the adequate functional space for the variational formulation of Maxwell's equations. Vector fields in such finite element (FE) spaces have continuous tangential traces, which is consistent with the physics. Therefore, the natural degrees of freedom for these elements are related to tangential traces along edges or faces. Here, we take the symmetric second order tetrahedral edge elements [23]. When the unknowns are ordered according to the reverse Cuthill-McKee (RCM) ordering [16], the profile of FE matrix is highly banded which improves the condition number of the FE coefficient matrix. The sparse large-scale linear system can be most efficiently solved if the zero elements of the coefficient matrix are not stored. We use the commonly used compressed row storage (CRS) format, which makes no assumptions about the sparsity structure of the matrix and does not store any unnecessary elements. In fact, from the variational formula of our direct problem (1.2.1), the coefficient matrix is complex symmetric. Hence, only the lower triangular portion of the matrix needs to be stored. Figure 1.1 shows a typical sparsity pattern of an FE matrix with 1820 unknowns from the symmetric second order edge element. Regarding the linear solver, either biconjugate gradient (BiCG)

or quasi-minimal residual (QMR) algorithms with diagonal preconditioning may be employed to solve the sparse, symmetric, and complex system of the equations. It appears for our experiments that the QMR is more efficient.

In the following, we present two numerical examples where the number of the incident wave  $m = 20$ , the incident latitudinal angle  $\theta = 0$ , and the incident longitudinal angle  $\phi_j = (j - 1) * 2\pi/m, j = 1, \dots, m$ . The relaxation parameter  $\beta_k$  is taken to be  $0.1/k$  for the tested examples. For stability analysis, some relative random noise is added to the data, i.e. the tangential trace of the electric field takes the form

$$\nu \times E|_S := (1 + \sigma \text{rand}) \cdot (\nu \times E|_S).$$

Here, rand gives uniformly distributed random numbers in  $[-1, 1]$ , and  $\sigma$  is a noise level parameter taken to be 0.02 in our numerical experiments. Define the relative error by

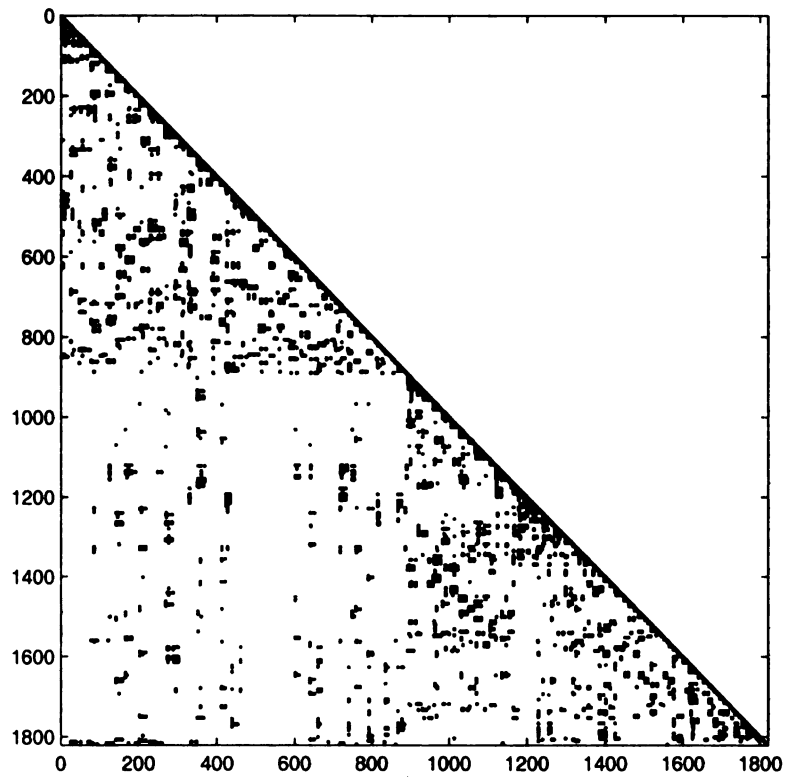
$$e_2 = \frac{(\sum_{i,j,k} |q_{ijk} - \bar{q}_{ijk}|^2)^{1/2}}{(\sum_{i,j,k} |q_{ijk}|^2)^{1/2}},$$

where  $\bar{q}$  is the reconstructed scatter and  $q$  is the true scatterer.

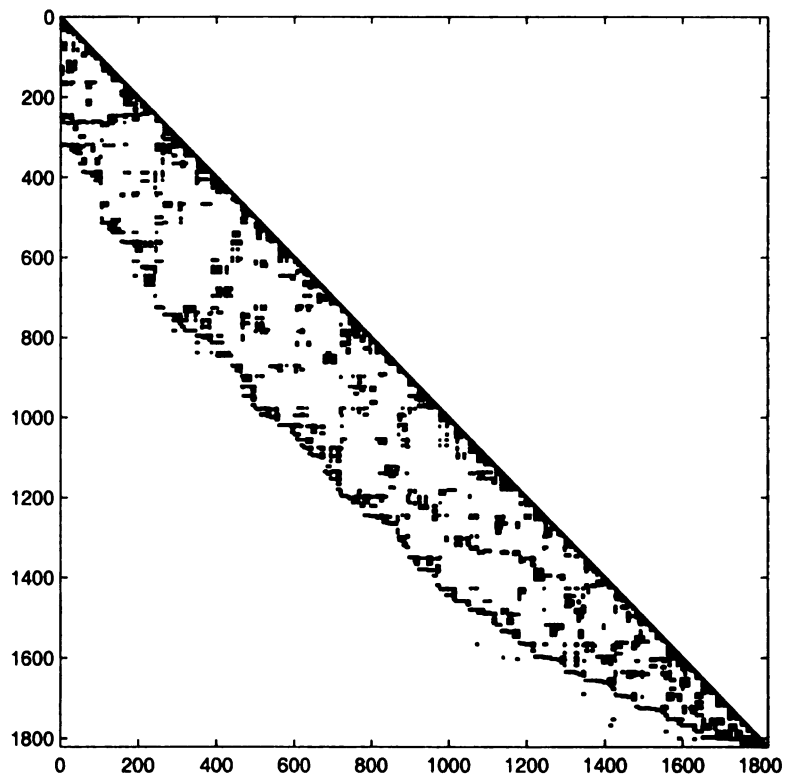
Example 1. Reconstruct a scatterer defined by

$$q(x, y, z) = \begin{cases} 1 - \sqrt{\frac{x^2}{1^2} + \frac{y^2}{0.8^2} + \frac{z^2}{0.5^2}} & \text{for } \frac{x^2}{1^2} + \frac{y^2}{0.8^2} + \frac{z^2}{0.5^2} \leq 1, \\ 0, & \text{otherwise.} \end{cases}$$

The compact support of this scatterer is an ellipsoid contained in the unit ball. For simplicity, we take  $\vec{n}_1 = \vec{n}_2$  and  $\vec{p}_1 = \vec{p}_2$  to test the forward solver. The numerical results are shown in Figure 1.2-1.4. In Figure 1.2, for the fixed incident latitudinal angle  $\theta = \pi/3$  and the longitudinal angle  $\phi = \pi/3$ , the forward problem is solved at different wavenumbers. In Figure 1.3 and 1.4, for the fixed wavenumber  $k = 2$ , the numerical results are shown with different latitudinal angles  $\theta \in [0, \pi]$  (fix  $\phi = \pi/3$ )



(a)



(b)

Figure 1.1. Parsity pattern of an FE matrix with 1820 unknowns: (a) original ordering; (b) RCM ordering.

$k$	1	2	3	4	5	6
$e_2$	0.5494	0.4876	0.3197	0.1856	0.1534	0.0895

Table 1.2. Relative error at different wavenumbers of Example 1.

and with different longitudinal angles  $\phi \in [0, 2\pi]$  (fix  $\theta = \pi/3$ ), respectively. It is easily seen from Figure 1.2 that the first term of the right-hand side of the integral equation (1.3.2) is dominant compared with the second (nonlinear) term when the wavenumber is small, which validates the Born approximation. Figure 1.5-1.7 (a) show the slices of the true scatterer and Figure 1.5-1.7 (b) give the reconstruction at the wavenumber  $k = 6$ . The relative errors are shown in Table 1.2 at different wavenumbers.

Example 2. Reconstruct a scatterer defined by

$$q(x, y, z) = \begin{cases} \sin\left(\frac{4\pi}{25}\right) - \sin\left((x^2 + (y + 0.5)^2 + z^2)\pi\right) & \text{for } x^2 + (y + 0.5)^2 + z^2 \leq 0.4^2, \\ \sin\left(\frac{4\pi}{25}\right) - \sin\left((x^2 + (y - 0.5)^2 + z^2)\pi\right) & \text{for } x^2 + (y - 0.5)^2 + z^2 \leq 0.4^2, \\ 0, & \text{otherwise.} \end{cases}$$

The compact support of this scatterer is two isolated balls with the same radius of 0.4 and the centers at  $(0, -0.5, 0)$  and  $(0, 0.5, 0)$ . For simplicity, we take  $\vec{n}_1 = \vec{n}_2$  and  $\vec{p}_1 = \vec{p}_2$  in the test of the forward solver. The numerical results are given in Figure 1.8-2.0. In Figure 1.8, for the fixed incident latitudinal angle  $\theta = \pi/3$  and the longitudinal angle  $\phi = \pi/3$ , the forward problem is solved at different wavenumbers. In Figure 1.9 and 2.0, for the fixed wavenumber  $k = 3$ , the numerical results are shown with different latitudinal angles  $\theta \in [0, \pi]$  (fix  $\phi = \pi/3$ ) and with different longitudinal angles  $\phi \in [0, 2\pi]$  (fix  $\theta = \pi/3$ ), respectively. It is easily seen from Figure 1.8 that the first term of the right-hand side of the integral equation (1.3.2) is dominant compared with the second (nonlinear) term when the wavenumber  $k$  is small, which once again

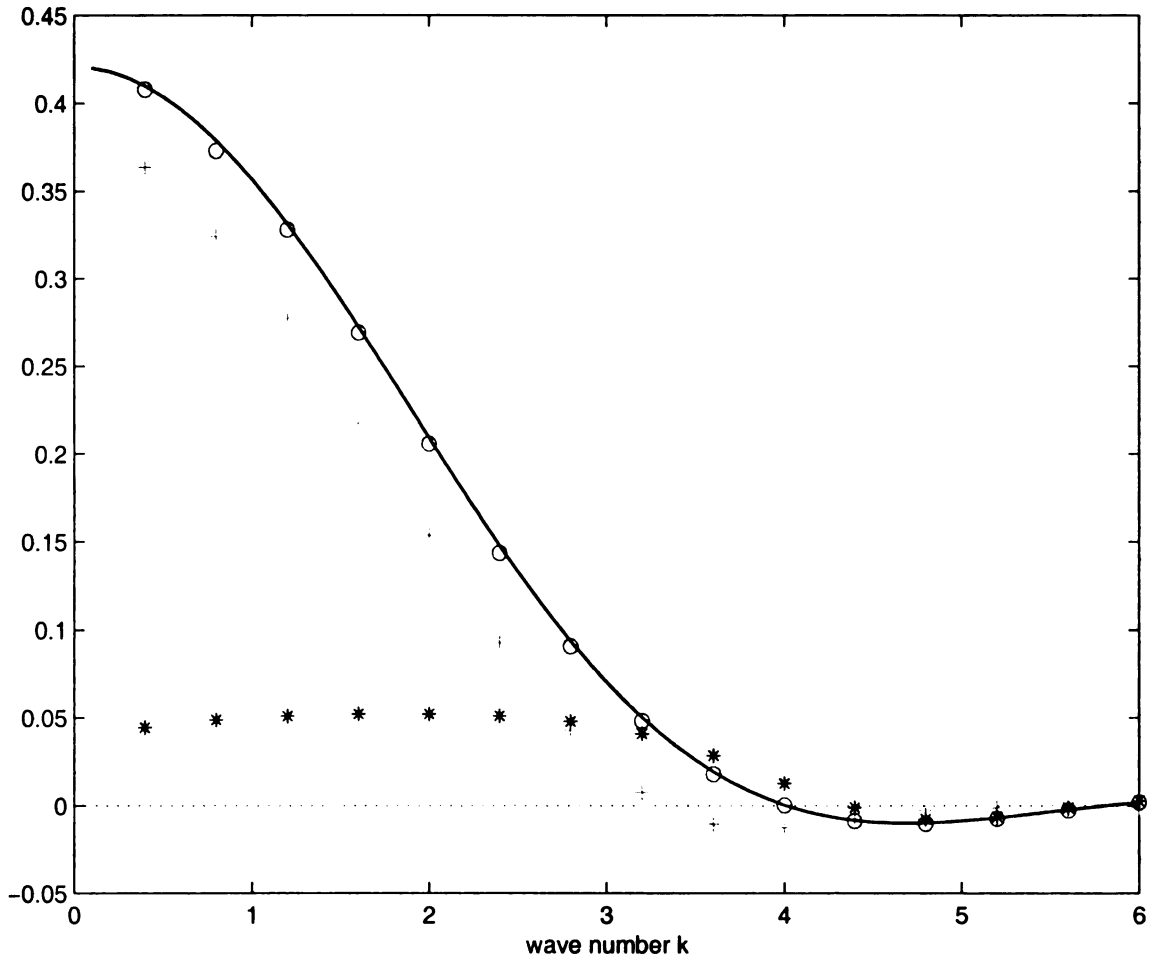


Figure 1.2. Example 1: Integrals at different wavenumbers for the fixed incident angle  $\theta = \pi/3$  and  $\phi = \pi/3$ . Solid curve: the exact integral value of the left-hand side of (1.3.2), +: the computed integral value of the first term of the right-hand side of (1.3.2), \*: the computed integral value of the second term of right-hand side of (1.3.2), o: the computed integral value of the right-hand side of (1.3.2).

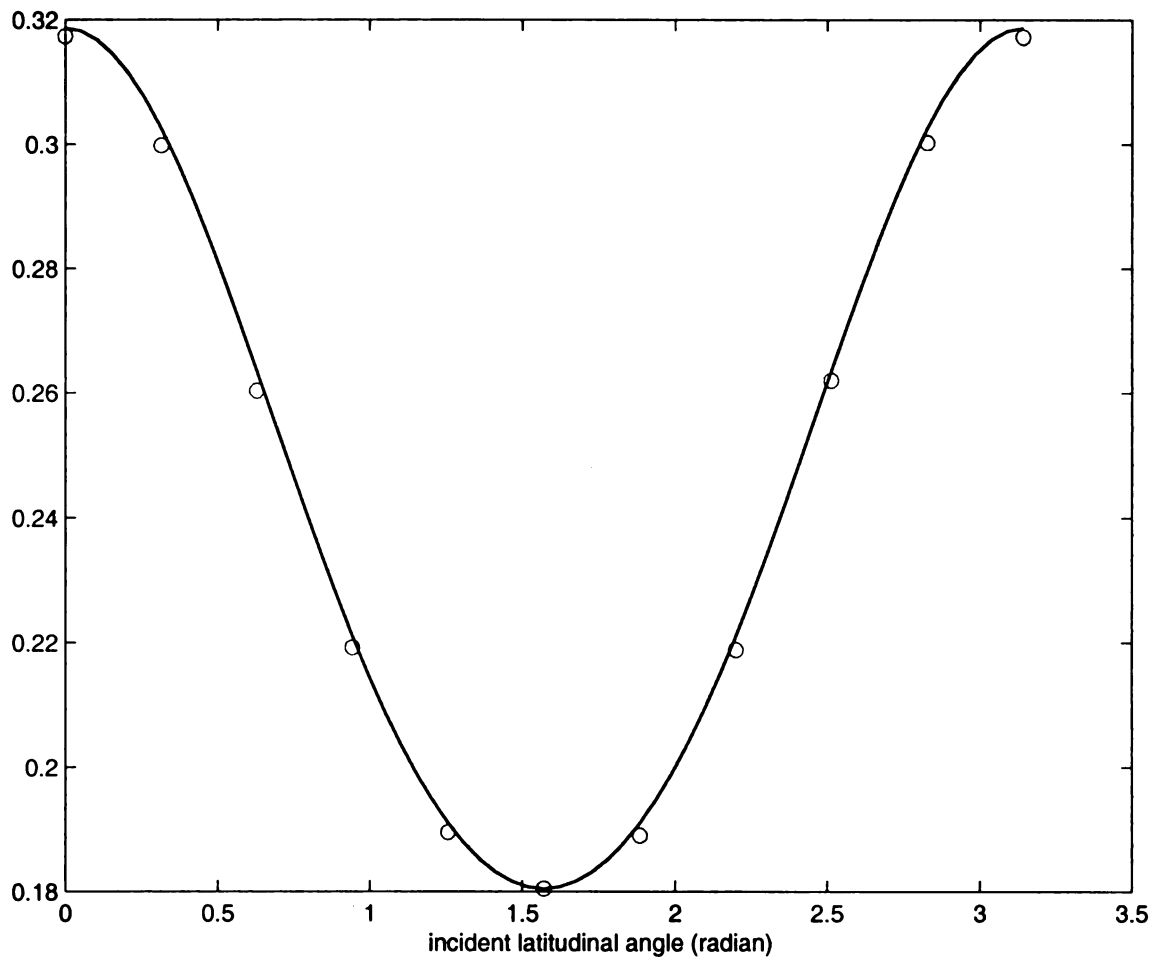


Figure 1.3. Example 1: Integrals with different  $\theta$  for the fixed wave number  $k = 2.0$  and  $\phi = \pi/3$ . Solid curve: the exact integral value of the left-hand side of (1.3.2),  $\circ$ : the computed integral value of the right hand-side of (1.3.2).

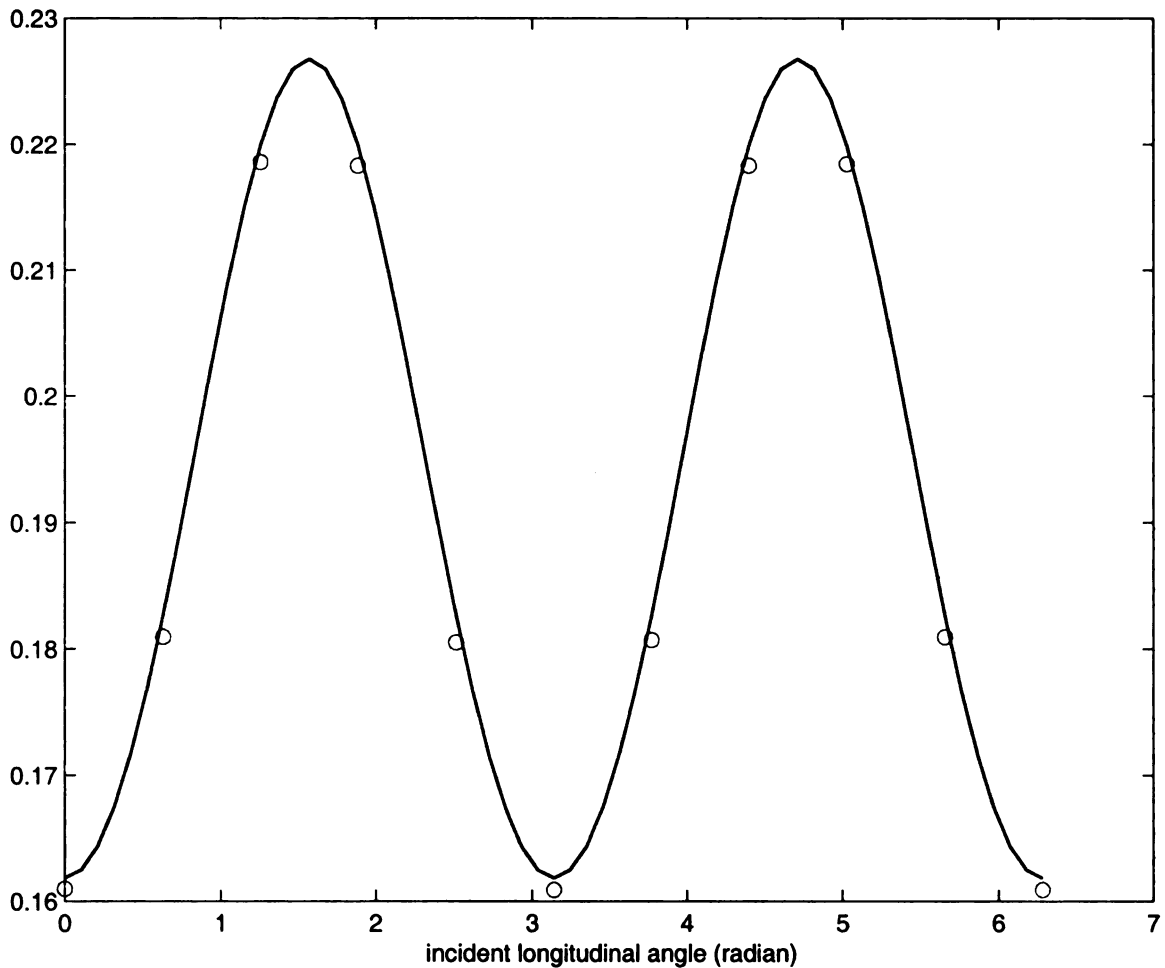


Figure 1.4. Example 1: Integrals with different  $\phi$  for the fixed wave number  $k = 2.0$  and  $\theta = \pi/3$ . Solid curve: the exact integral value of the left-hand side of (1.3.2),  $\circ$ : the computed integral value of the right-hand side of (1.3.2).

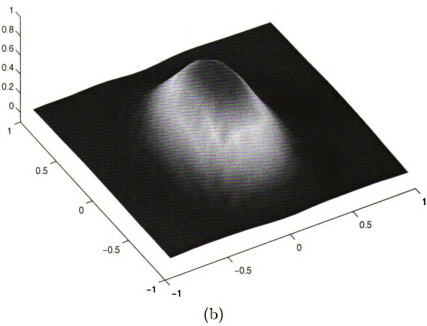
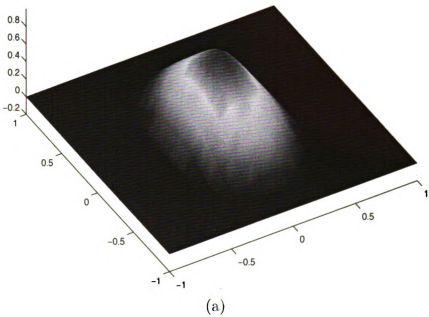


Figure 1.5. Example 1: (a) the slice  $x = 0$  of the true scatterer; (b) the slice  $x = 0$  of the reconstruction.

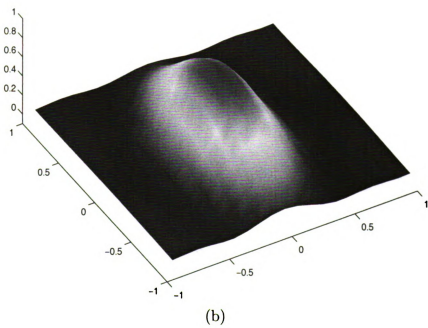
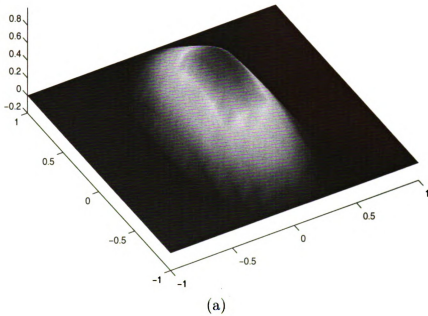


Figure 1.6. Example 1: (a) the slice  $y = 0$  of the true scatterer; (b) the slice  $y = 0$  of the reconstruction.

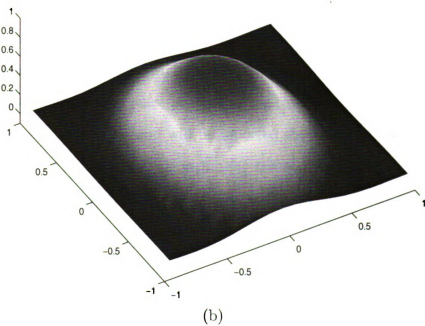
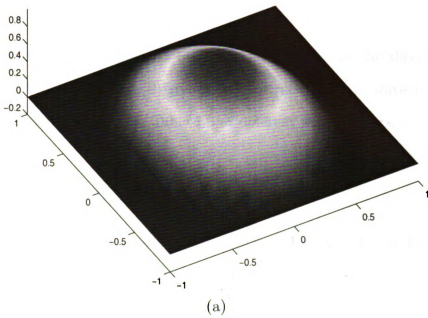


Figure 1.7. Example 1: (a) the slice  $z = 0$  of the true scatterer; (b) the slice  $z = 0$  of the reconstruction.

$k$	1	2	3	4	5	6	7
$e_2$	0.6963	0.6479	0.5891	0.4951	0.3376	0.2568	0.2221

Table 1.3. Relative error at different wavenumbers of Example 2.

validates the Born approximation. Figure 1.11-1.13 (a) show the slices of the true scatterer, and Figure 1.11-1.13 (b) give the reconstruction at the wavenumber  $k = 7$ . The relative errors are shown in Table 1.3 at different wavenumbers.

## 1.5 Concluding Remarks

The proposed recursive linearization algorithm is stable and efficient for solving the inverse medium scattering problem with multiple frequency scattering data in three dimensions. Theoretically, scattering data with even higher-wavenumbers could be used to recover more complicated scatterers which contain higher frequency features, i.e. more Fourier modes. However, the difficulty lies in the fact that the forward model becomes difficult to solve due to the highly oscillatory nature of the solution. For a larger  $k$ , the mesh size has to be smaller, which makes numerical solution more expensive. Finally, we point out two important future directions of this research. The first concerns with the convergence analysis of the recursive linearization algorithm, which is currently in progress and will be reported elsewhere. Another challenging project is to develop an efficient algorithm for the inverse medium scattering with fixed frequency scattering data.

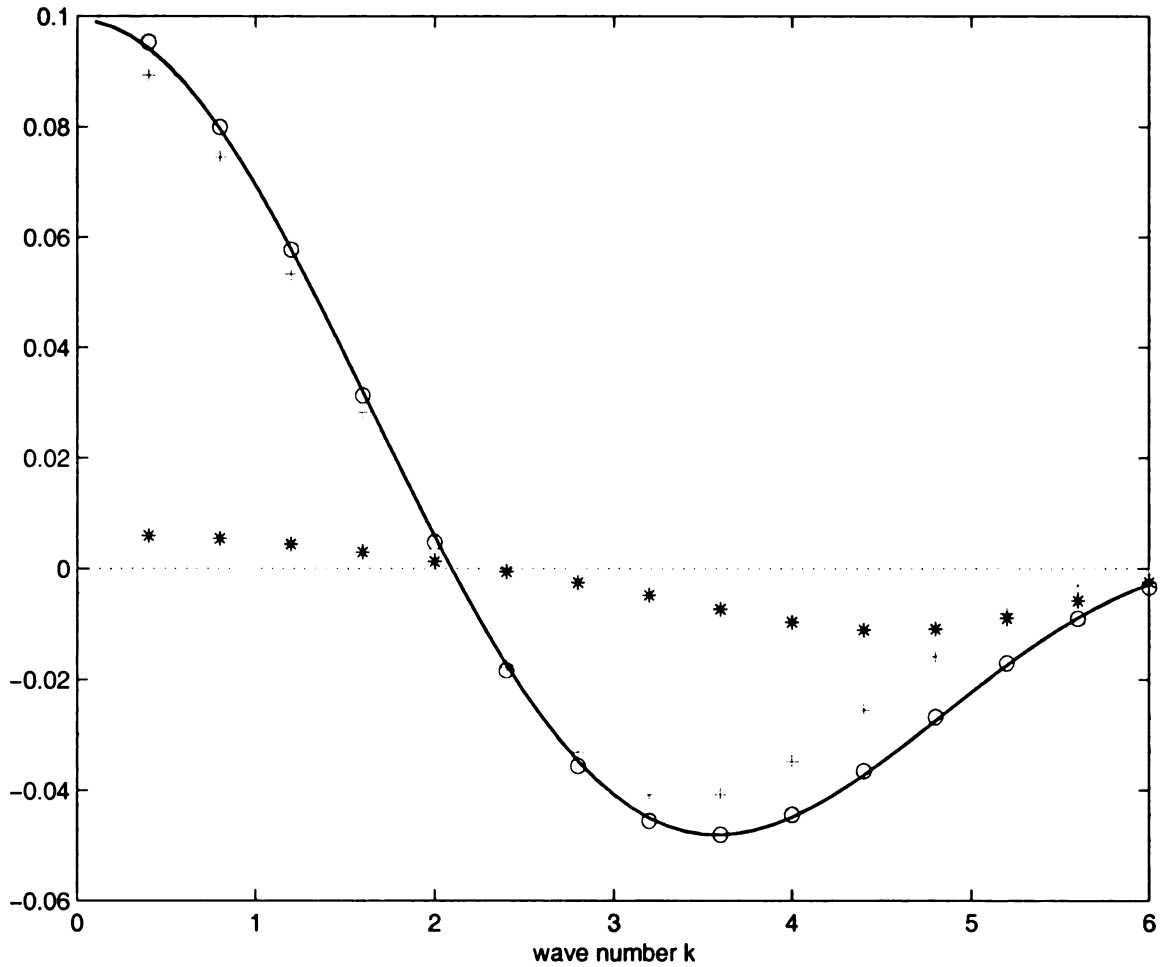


Figure 1.8. Example 2: Integrals at different wavenumbers for the fixed incident angle  $\theta = \pi/3$  and  $\phi = \pi/3$ . Solid curve: the exact integral value of the left-hand side of (1.3.2), +: the computed integral value of the first term of the right-hand side of (1.3.2), \*: the computed integral value of the second term of right-hand side of (1.3.2), o: the computed integral value of the right-hand side of (1.3.2).

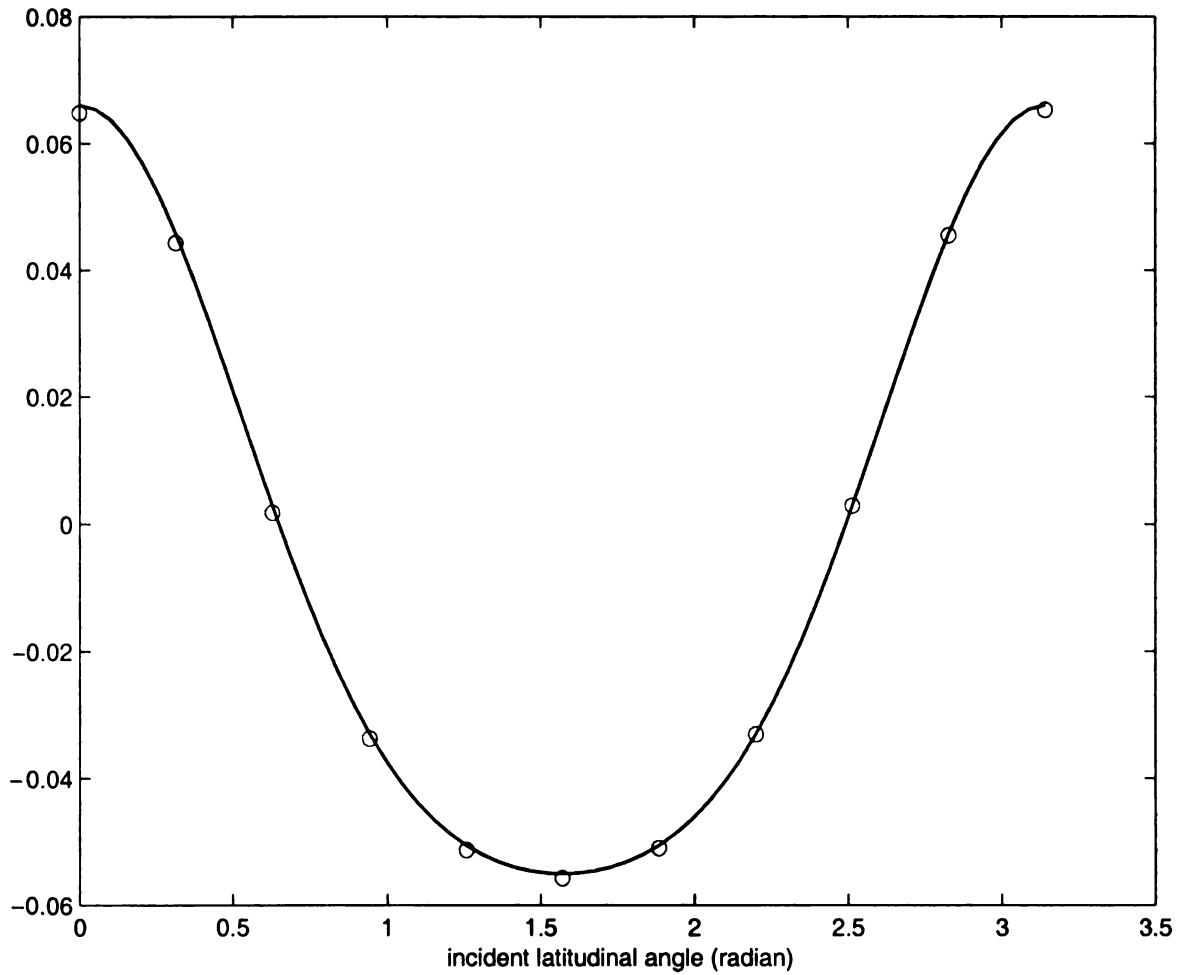


Figure 1.9. Example 2: Integrals with different  $\theta$  for the fixed wave number  $k = 3.0$  and  $\phi = \pi/3$ . Solid curve: the exact integral value of the left-hand side of (1.3.2),  $\circ$ : the computed integral value of the right hand-side of (1.3.2).

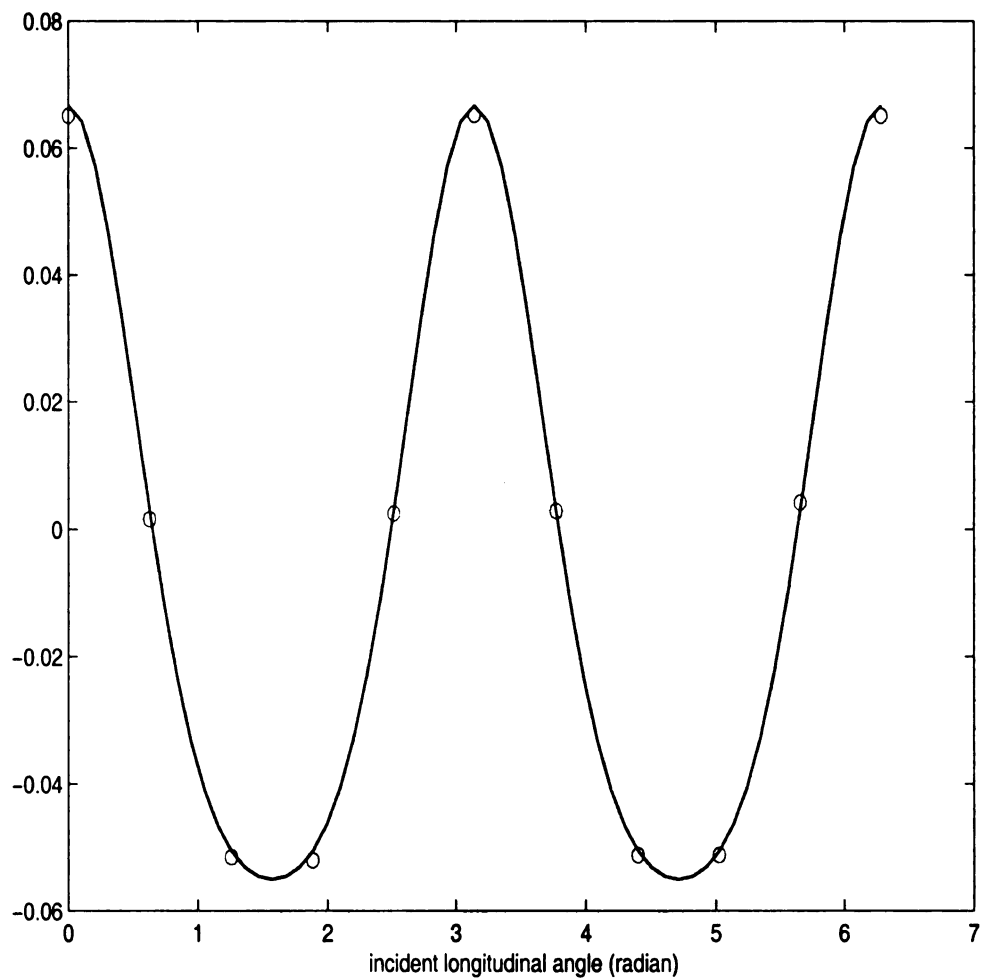


Figure 1.10. Example 2: Integrals with different  $\phi$  for the fixed wave number  $k = 2.0$  and  $\theta = \pi/3$ . Solid curve: the exact integral value of the left-hand side of (1.3.2),  $\circ$ : the computed integral value of the right-hand side of (1.3.2).

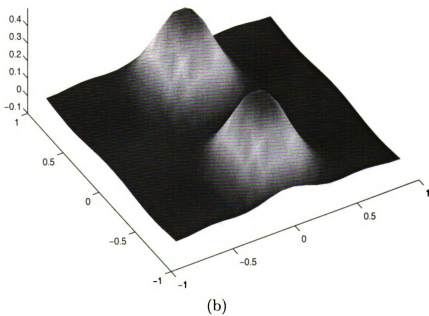
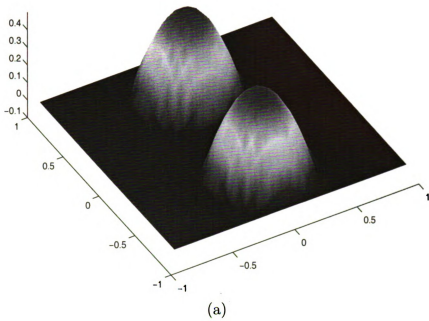


Figure 1.11. Example 2: (a) the slice  $x = 0$  of the true scatterer; (b) the slice  $x = 0$  of the reconstruction.

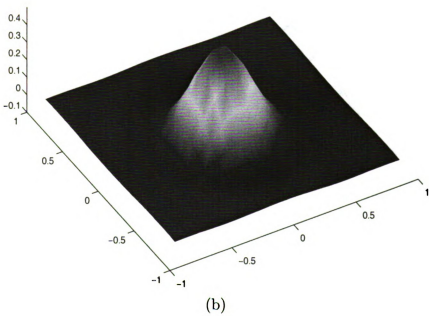
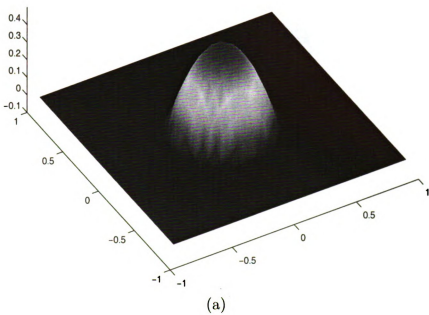


Figure 1.12. Example 2: (a) the slice  $y = -0.5$  of the true scatterer; (b) the slice  $y = -0.5$  of the reconstruction.

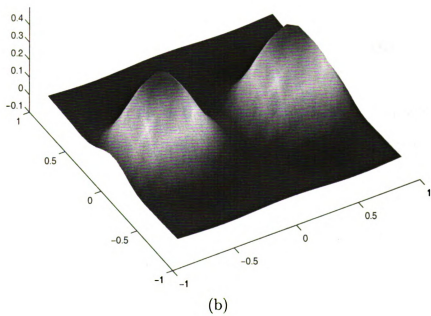
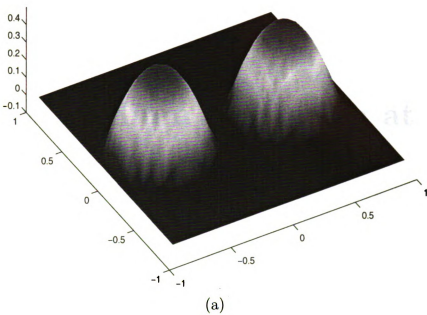


Figure 1.13. Example 2: (a) the slice  $z = 0$  of the true scatterer; (b) the slice  $z = 0$  of the reconstruction.

# CHAPTER 2

## Inverse Medium Scattering at Fixed Frequency

### 2.1 Introduction

Consider the Helmholtz equation in two dimensions

$$\Delta\phi + k_0^2(1 + q(x))\phi = 0, \quad (2.1.1)$$

where  $\phi$  is the total field;  $k_0$  is the wavenumber, and  $q(x) > -1$ , which has a compact support and a lower bound, is the scatterer.

Assume that the scatterer lies in the upper half plane  $\mathbb{R}_+^2 = \{(x_1, x_2) \in \mathbb{R}^2 : x_2 > 0\}$ . Denote the wave vector  $\mathbf{k} = (\eta, k(\eta))$ , where  $\eta$  is the transverse part of the wave vector and

$$k(\eta) = \begin{cases} \sqrt{k_0^2 - \eta^2} & \text{for } k_0 \geq |\eta|, \\ i\sqrt{\eta^2 - k_0^2} & \text{for } k_0 < |\eta|. \end{cases}$$

The number  $|\eta|$  is known as the spatial frequency.

The scatterer is illuminated by a one-parameter family of plane waves

$$\phi_0 = e^{i\mathbf{k} \cdot \mathbf{x}}, \quad (2.1.2)$$

which gives explicitly

$$\phi_0(x_1, x_2) = \begin{cases} e^{i(\eta x_1 + \sqrt{k_0^2 - \eta^2} x_2)} & \text{for } k_0 \geq |\eta|, \\ e^{i\eta x_1 - \sqrt{\eta^2 - k_0^2} x_2} & \text{for } k_0 < |\eta|. \end{cases}$$

The modes for which  $|\eta| \leq k_0$  correspond to propagating plane waves while the modes with  $|\eta| > k_0$  correspond to evanescent plane waves. Therefore, the illuminating field could consist of high spatial frequency evanescent plane waves. They may be generated at the interface of two media by total internal reflection [12, 18], which has been in practical use for decades and primarily been used in near-field optics [6, 7]. A recent review on the near-field microscopy and near-field optics may be found in [11]. These waves are oscillatory parallel to the  $x_1$  axis and decay exponentially along the  $x_2$  axis in the upper half plane  $\mathbb{R}_+^2$ . The higher the spatial frequency of the evanescent plane waves used to probe the scatterer is, the more rapidly the field decays as a function of depth into the scatterer. See Figure 2.1 and 2.2 for examples. Evidently, such incident waves satisfy the homogeneous equation

$$\Delta\phi_0 + k_0^2\phi_0 = 0. \quad (2.1.3)$$

The total electric field  $\phi$  consists of the incident field  $\phi_0$  and the scattered field  $\psi$ :

$$\phi = \phi_0 + \psi.$$

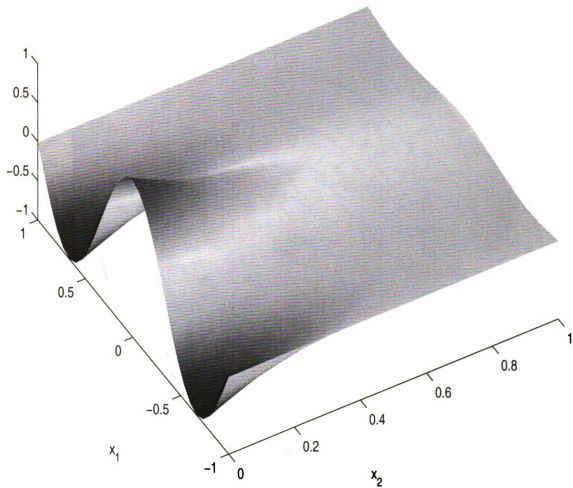


Figure 2.1. Evanescent plane wave at  $k_0 = 4.0$  with  $\eta = 4.7$ .

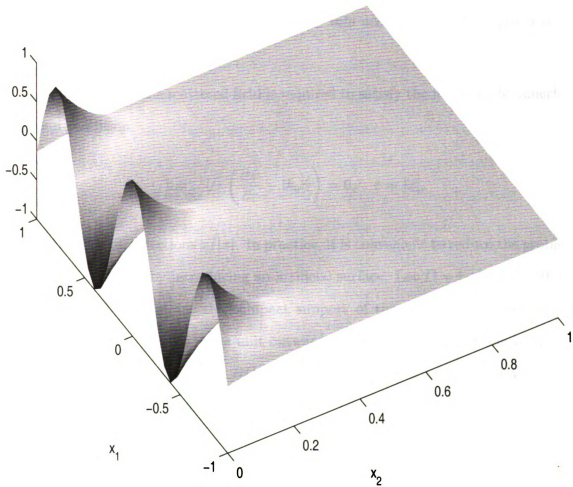


Figure 2.2. Evanescent plane wave at  $k_0 = 4.0$  with  $\eta = 8.0$ .

It follows from the equations (2.1.1) and (2.1.3) that the scattered field satisfies

$$\Delta\psi + k_0^2(1 + q)\psi = -k_0^2q\phi_0. \quad (2.1.4)$$

**Remark 2.1.1.** *In this paper, we adopt the non-global approach, i.e. the scattered field resulting from the interaction of the incident field with the scatterer is analyzed in the absence of other medium or tip. The scattering problem may be formulated in the free space. The global approach which takes into account the entire system is the subject of our ongoing research.*

In the free space, the scattered field is required to satisfy the following Sommerfeld radiation condition

$$\lim_{r \rightarrow \infty} \sqrt{r} \left( \frac{\partial\psi}{\partial r} - ik_0\psi \right) = 0, \quad r = |x|,$$

uniformly along all directions  $x/|x|$ . In practice, it is convenient to reduce the problem to a bounded domain by introducing an artificial surface. Let  $D = [-L_1, L_1] \times [0, L_2]$  be a square, which contains the compact support of the scatterer,  $\Omega$ . Let  $\partial D$  be the boundary of  $D$ . Denote  $n$  the unit outward normal to  $\partial D$ . A suitable boundary condition needs to be imposed on  $\partial D$ . For the sake of simplicity, we employ the first order absorbing boundary condition [22] as

$$\frac{\partial\psi}{\partial n} - ik_0\psi = 0, \quad \text{on } \partial D. \quad (2.1.5)$$

Given the incident field  $\phi_0$ , the direct problem is to determine the scattered field  $\psi$  for the known scatterer  $q(x)$ . Using the Lax-Milgram lemma and the Fredholm alternative, the direct problem is shown in this paper to have a unique solution for all  $k_0 > 0$ . An energy estimate for the scattered field is given, which provides a criterion for the weak scattering. Furthermore, properties on the continuity and the Fréchet

differentiability of the nonlinear scattering map are examined. For the regularity analysis of the scattering map in an open domain, the reader is referred to [2, 24, 10]. The inverse medium scattering problem is to determine the scatterer  $q(x)$  from the measurements of near-field currents densities,  $\psi|_{\partial D}$ , given the incident field  $\phi_0$ . The inverse medium scattering problems arise naturally in diverse applications such as radar, sonar, geophysical exploration, medical imaging, and nondestructive testing [10]. However, there are two major difficulties associated with these inverse problems: the ill-posedness and the presence of many local minima. In [8, 4], stable and efficient continuation methods with respect to the wavenumber were proposed to solve the two-dimensional Helmholtz equation and the three-dimensional Maxwell's equations, respectively, in the case of full aperture data. A homotopy continuation method with limited aperture data may be found in [3]. These approaches require multi-frequency scattering data and are based on recursive linearization along wavenumbers.

The main purpose of this paper is to study the inverse medium problem for Helmholtz's equations at a single-frequency. We present a new continuation method for the inverse medium scattering problem. In the case of radially symmetric scatterers, Chen in [9] developed a recursive linearization algorithm with single-frequency data, where spherical incident waves were used. In this paper, we attempt to remove the radially symmetric assumption on the medium. Our approach is motivated by the recent studies of near-field optics. As a special feature, the illuminating fields used in this paper including the high spatial frequency evanescent plane waves are a one-parameter family of plane waves. When a medium is probed with an evanescent plane wave at a high spatial frequency, only a thin layer of the medium is penetrated. Corresponding to this exponentially decaying incident field, the scattered field measured on the boundary contains information of the medium in that thin layer. Although such a measurement is entirely inadequate to determine the whole medium, it does give rise to an approximation. To accurately determine the medium, information

at lower spatial frequencies of the evanescent plane waves is needed to illuminate the medium. While the probing field penetrates a thicker layer of the medium, the relation between the measurement and the scatterer to be recovered in the thicker layer becomes more nonlinear. These nonlinear equations can be considered as perturbations to the already solved equations in the previous thicker layers. Therefore, they can be continually and recursively linearized by a standard perturbation technique. Thus, the recursive linearization is a continuation method along the transverse direction of the incident wave, which controls the depth of its penetration.

The plan of this paper is as follows. The analysis of the variational problem for direct scattering is presented in Section 2.2. In particular, the well-posedness of the direct scattering is proved. The Fréchet differentiability of the scattering map is also given. In Section 2.3, an initial guess of the reconstruction from the Born approximation is derived in the case of weak scattering. Section 2.4 is devoted to numerical study of a regularized iterative linearization algorithm. Numerical examples are presented. The paper is concluded with some general remarks and directions for future research in Section 2.5.

## 2.2 Analysis of the Scattering Map

In this section, the direct scattering problem is studied to provide some criterion for the weak scattering, which plays an important role in the inversion method. The Fréchet differentiability of the scattering map for the problem (2.1.4), (2.1.5) is examined.

**Remark 2.2.1.** *Some analysis of the scattering map was given previously by Keys and Weglein [24] based on the integral equation approach and contraction mapping theorem. The assumption of small perturbation of the potential is necessary for their approach. Our approach is different. Based on the Fredholm alternative and a unique-*

ness result, we develop a variational approach to prove the existence of the scattered field for all  $k_0 > 0$ , given  $q \in L^\infty(D)$ , the continuity of the scattering map, the boundedness of the formal linearized map, and the Fréchet differentiability of the scattering map. The assumption of small perturbation is not needed in our analysis. More importantly, we give an explicit energy estimate for the scattered field, which provides a criterion for weak scattering hence plays a central role in the development of the inversion algorithm of Section 2.3. An analysis of the Fréchet differentiability on the scattering map for the equation (2.1.4) along with the Sommerfeld radiation condition may also be found in [2] using the integral equation approach.

To state our boundary value problem, we introduce the bilinear form  $a : H^1(D) \times H^1(D) \rightarrow \mathbb{C}$

$$a(u, v) = (\nabla u, \nabla v) - k_0^2((1 + q)u, v) - ik_0\langle u, v \rangle,$$

and the linear functional on  $H^1(D)$

$$b(v) = k_0^2(q\phi_0, v).$$

Here, we have used the standard inner products

$$(u, v) = \int_D u \cdot \bar{v} dx \text{ and } \langle u, v \rangle = \int_{\partial D} u \cdot \bar{v} ds,$$

where the overline denotes the complex conjugate.

Then, we have the weak form of the boundary value problem (2.1.4) and (2.1.5): find  $\psi \in H^1(D)$  such that

$$a(\psi, \xi) = b(\xi), \quad \forall \xi \in H^1(D). \tag{2.2.1}$$

Throughout the paper, the constant  $C$  stands for a positive generic constant whose

value may change step by step, but should always be clear from the contexts.

For a given scatterer  $q$  and an incident field  $\phi_0$ , we define the map  $S(q, \phi_0)$  by  $\psi = S(q, \phi_0)$ , where  $\psi$  is the solution of the problem (2.1.4), (2.1.5) or the variational problem (2.2.1). It is easily seen that the map  $S(q, \phi_0)$  is linear with respect to  $\phi_0$  but is nonlinear with respect to  $q$ . Hence, we may denote  $S(q, \phi_0)$  by  $S(q)\phi_0$ .

Concerning the map  $S(q)$ , we have the following regularity results. Lemma 2.2.3 gives the boundedness of  $S(q)$ , while a continuity result for the map  $S(q)$  is presented in Lemma 2.2.4.

**Lemma 2.2.1.** *Given the scatterer  $q \in L^\infty(D)$ , the direct scattering problem (2.1.4), (2.1.5) has at most one solution.*

PROOF. It suffices to show that  $\psi = 0$  in  $D$  if  $\phi_0 = 0$  (no source term). From the Green's formula

$$0 = \int_D (\psi \Delta \bar{\psi} - \bar{\psi} \Delta \psi) dx = \int_{\partial D} (\psi \frac{\partial \bar{\psi}}{\partial n} - \bar{\psi} \frac{\partial \psi}{\partial n}) ds = -2ik_0 \int_{\partial D} |\psi|^2 ds,$$

we get  $\psi = 0$  on  $\partial D$ . The absorbing boundary condition on  $\partial D$  yields further that  $\frac{\partial \psi}{\partial n} = 0$  on  $\partial D$ . By the Holmgren uniqueness theorem,  $\psi = 0$  in  $\mathbb{R}^2 \setminus D$ . A unique continuation result [21] concludes that  $\psi = 0$  in  $D$ .  $\square$

**Lemma 2.2.2.** *If the wavenumber  $k_0$  is sufficiently small, the variational problem (2.2.1) admits a unique weak solution in  $H^1(D)$  and  $S(q)$  is a bounded linear map from  $L^2(D)$  to  $H^1(D)$ . Furthermore, there is a constant  $C$  dependent of  $D$ , such that*

$$\| S(q)\phi_0 \|_{H^1(D)} \leq C k_0 \| q \|_{L^\infty(D)} \| \phi_0 \|_{L^2(D)}. \quad (2.2.2)$$

PROOF. Decompose the bilinear form  $a$  into  $a = a_1 + k_0^2 a_2$ , where

$$a_1(\psi, \xi) = (\nabla \psi, \nabla \xi) - ik_0 \langle \psi, \xi \rangle,$$

$$a_2(\psi, \xi) = -((1 + q)\psi, \xi).$$

We conclude that  $a_1$  is coercive from

$$\begin{aligned} |a_1(\psi, \psi)| &\geq C(\|\nabla \psi\|_{L^2(D)}^2 + k_0 \|\psi\|_{H^{1/2}(\partial D)}^2) \\ &\geq Ck_0(\|\nabla \psi\|_{L^2(D)}^2 + \|\psi\|_{H^{1/2}(\partial D)}^2) \\ &\geq Ck_0 \|\psi\|_{H^1(D)}^2, \end{aligned}$$

where the last inequality may be obtained by applying standard elliptic estimates [17]. Next, we prove the compactness of  $a_2$ . Define an operator  $\mathcal{A} : L^2(D) \rightarrow H^1(D)$  by

$$a_1(\mathcal{A}\psi, \xi) = a_2(\psi, \xi), \quad \forall \xi \in H^1(D),$$

which gives

$$(\nabla \mathcal{A}\psi, \nabla \xi) - ik_0 \langle \mathcal{A}\psi, \xi \rangle = -((1 + q)\psi, \xi), \quad \forall \xi \in H^1(D).$$

Using the Lax–Milgram Lemma, it follows that

$$\|\mathcal{A}\psi\|_{H^1(D)} \leq \frac{C}{k_0} \|\psi\|_{L^2(D)}, \quad (2.2.3)$$

where the constant  $C$  is independent of  $k_0$ . Thus  $\mathcal{A}$  is bounded from  $L^2(D)$  to  $H^1(D)$  and  $H^1(D)$  is compactly imbedded into  $L^2(D)$ . Hence  $\mathcal{A} : L^2(D) \rightarrow L^2(D)$  is a compact operator.

Define a function  $u \in L^2(D)$  by requiring  $u \in H^1(D)$  and satisfying

$$a_1(u, \xi) = b(\xi), \quad \forall \xi \in H^1(D).$$

It follows from the Lax–Milgram Lemma again that

$$\|u\|_{H^1(D)} \leq C k_0 \|q\|_{L^\infty(D)} \|\phi_0\|_{L^2(D)}. \quad (2.2.4)$$

Using the operator  $\mathcal{A}$ , we can see that the problem (2.2.1) is equivalent to find  $\psi \in L^2(D)$  such that

$$(\mathcal{I} + k_0^2 \mathcal{A})\psi = u. \quad (2.2.5)$$

When the wavenumber  $k_0$  is small enough, the operator  $\mathcal{I} + k_0^2 \mathcal{A}$  has a uniformly bounded inverse. We then have the estimate

$$\|\psi\|_{L^2(D)} \leq C \|u\|_{L^2(D)}, \quad (2.2.6)$$

where the constant  $C$  is independent of  $k_0$ . Rearranging (2.2.5), we have  $\psi = u - k_0^2 \mathcal{A}\psi$ , so  $\psi \in H^1(D)$  and, by the estimate (2.2.3) for the operator  $\mathcal{A}$ , we have

$$\|\psi\|_{H^1(D)} \leq \|u\|_{H^1(D)} + C k_0 \|\psi\|_{L^2(D)}.$$

The proof is complete by combining the estimates (2.2.6) and (2.2.4) and observing that  $\psi = S(q)\phi_0$ .  $\square$

For a general wavenumber  $k_0 > 0$ , from the equation (2.2.5), the existence follows from the Fredholm alternative and the uniqueness result. However, the constant  $C$  in the estimate (2.2.2) depends on the wavenumber.

**Lemma 2.2.3.** *Given the scatterer  $q \in L^\infty(D)$ , the variational problem (2.2.1) admits*

a unique weak solution in  $H^1(D)$  for all  $k_0 > 0$  and  $S(q)$  is a bounded linear map from  $L^2(D)$  to  $H^1(D)$ . Furthermore, it holds the estimate

$$\| S(q)\phi_0 \|_{H^1(D)} \leq C \| q \|_{L^\infty(D)} \| \phi_0 \|_{L^2(D)}, \quad (2.2.7)$$

where the constant  $C$  depends on  $k_0$  and  $D$ .

**Remark 2.2.2.** It follows from the explicit form of the incident field (2.1.2) and the estimate (2.2.7) that

$$\| \psi \|_{H^1(D)} \leq C |\Omega|^{1/2} \| q \|_{L^\infty(D)},$$

where  $\Omega$  is the compact support of the scatterer  $q$  and the constant  $C$  depends on  $k_0, D$ . Moreover, we have for  $|\eta| > k_0$  that

$$\| \psi \|_{H^1(D)} \leq C (\eta^2 - k_0^2)^{-1/4} \| q \|_{L^\infty(D)}, \quad (2.2.8)$$

where the constant  $C$  depends on  $k_0$  and  $D$ .

**Remark 2.2.3.** The estimate of the scattered field in Remark 2.2.1 provides a criterion for the weak scattering. For a fixed wavenumber  $k_0$  and a scatterer  $q$ , the scattered field is weak if the spatial frequency of the incident wave,  $|\eta|$ , is large.

**Lemma 2.2.4.** Assume that  $q_1, q_2 \in L^\infty(D)$ . Then

$$\| S(q_1)\phi_0 - S(q_2)\phi_0 \|_{H^1(D)} \leq C \| q_1 - q_2 \|_{L^\infty(D)} \| \phi_0 \|_{L^2(D)}, \quad (2.2.9)$$

where the constant  $C$  depends on  $k_0, D$ , and  $\| q_2 \|_{L^\infty(D)}$ .

**PROOF.** Let  $\psi_1 = S(q_1)\phi_0$  and  $\psi_2 = S(q_2)\phi_0$ . It follows that for  $j = 1, 2$

$$\Delta \psi_j + k_0^2 (1 + q_j) \psi_j = -k_0^2 q_j \phi_0.$$

By setting  $w = \psi_1 - \psi_2$ , we have

$$\Delta w + k_0^2(1 + q_1)w = -k_0^2(q_1 - q_2)(\phi_0 + \psi_2).$$

The function  $w$  also satisfies the boundary condition (2.1.5).

We repeat the procedure in the proof of Lemma 2.2.3 to obtain

$$\|w\|_{H^1(D)} \leq C \|q_1 - q_2\|_{L^\infty(D)} \|\phi_0 + \psi_2\|_{L^2(D)}.$$

Using Lemma 2.2.3 again for  $\psi_2$  yields

$$\|\psi_2\|_{H^1(D)} \leq C \|q_2\|_{L^\infty(D)} \|\phi_0\|_{L^2(D)},$$

which gives

$$\|S(q_1)\phi_0 - S(q_2)\phi_0\|_{H^1(D)} \leq C \|q_1 - q_2\|_{L^\infty(D)} \|\phi_0\|_{L^2(D)},$$

where the constant  $C$  depends on  $D, k_0$ , and  $\|q_2\|_{L^\infty(D)}$ . □

Let  $\gamma$  be the restriction (trace) operator to the boundary  $\partial D$ . By the trace theorem,  $\gamma$  is a bounded linear operator from  $H^1(D)$  onto  $H^{1/2}(\partial D)$ . We can now define the scattering map  $M(q) = \gamma S(q)$ .

Next, consider the Fréchet differentiability of the scattering map. Recall the map  $S(q)$  is nonlinear with respect to  $q$ . Formally, by using the first order perturbation theory, we obtain the linearized scattering problem of (2.1.4), (2.1.5) with respect to a reference scatterer  $q$ ,

$$\Delta v + k_0^2(1 + q)v = -k_0^2\delta q(\phi_0 + \psi), \tag{2.2.10}$$

$$\frac{\partial v}{\partial n} - ik_0v = 0, \tag{2.2.11}$$

where  $\psi = S(q)\phi_0$ .

Define the formal linearization  $T(q)$  of the map  $S(q)$  by  $v = T(q)(\delta q, \phi_0)$ , where  $v$  is the solution of the problem (2.2.10), (2.2.11). The following is a boundedness result for the map  $T(q)$ . A proof may be given by following step by step the proofs of Lemma 2.2.2 and Lemma 2.2.3. Hence we omit it here.

**Lemma 2.2.5.** *Assume that  $q, \delta q \in L^\infty(D)$  and  $\phi_0$  is the incident field. Then  $v = T(q)(\delta q, \phi_0) \in H^1(D)$  with the estimate*

$$\|T(q)(\delta q, \phi_0)\|_{H^1(D)} \leq C \|\delta q\|_{L^\infty(D)} \|\phi_0\|_{L^2(D)}, \quad (2.2.12)$$

where the constant  $C$  depends on  $k_0, D$ , and  $\|q\|_{L^\infty(D)}$ .

The next lemma is concerned with the continuity property of the map.

**Lemma 2.2.6.** *For any  $q_1, q_2 \in L^\infty(D)$  and an incident field  $\phi_0$ , the following estimate holds*

$$\|T(q_1)(\delta q, \phi_0) - T(q_2)(\delta q, \phi_0)\|_{H^1(D)} \leq C \|q_1 - q_2\|_{L^\infty(D)} \|\delta q\|_{L^\infty(D)} \|\phi_0\|_{L^2(D)}, \quad (2.2.13)$$

where the constant  $C$  depends on  $k_0, D$ , and  $\|q_2\|_{L^\infty(D)}$ .

**PROOF.** Let  $v_i = T(q_i)(\delta q, \phi_0)$ , for  $i = 1, 2$ . It is easy to see that

$$\begin{aligned} \Delta(v_1 - v_2) + k_0^2(1 + q_1)(v_1 - v_2) = \\ - k_0^2 \delta q (\psi_1 - \psi_2) - k_0^2 (q_1 - q_2) v_2, \end{aligned}$$

where  $\psi_i = S(q_i)\phi_0$ .

Similar to the proof of Lemma 2.2.3, we get

$$\|v_1 - v_2\|_{H^1(D)} \leq C \left( \|\delta q\|_{L^\infty(D)} \|\psi_1 - \psi_2\|_{H^1(D)} + \|q_1 - q_2\|_{L^\infty(D)} \|v_2\|_{H^1(D)} \right).$$

From Lemma 2.2.2 and Lemma 2.2.3, we obtain

$$\|v_1 - v_2\|_{H^1(D)} \leq C \|q_1 - q_2\|_{L^\infty(D)} \|\delta q\|_{L^\infty(D)} \|\phi_0\|_{L^2(D)},$$

which completes the proof.  $\square$

The following result concerns the differentiability property of  $S(q)$ .

**Lemma 2.2.7.** *Assume that  $q, \delta q \in L^\infty(D)$ . Then there is a constant  $C$  dependent of  $k_0, D$ , and  $\|q\|_{L^\infty(D)}$ , for which the following estimate holds*

$$\|S(q + \delta q)\phi_0 - S(q)\phi_0 - T(q)(\delta q, \phi_0)\|_{H^1(D)} \leq C \|\delta q\|_{L^\infty(D)}^2 \|\phi_0\|_{L^2(D)}. \quad (2.2.14)$$

*Proof.* By setting  $\psi_1 = S(q)\phi_0$ ,  $\psi_2 = S(q + \delta q)\phi_0$ , and  $v = T(q)(\delta q, \phi_0)$ , we have

$$\begin{aligned} \Delta\psi_1 + k_0^2(1+q)\psi_1 &= -k_0^2q\phi_0, \\ \Delta\psi_2 + k_0^2(1+q+\delta q)\psi_2 &= -k_0^2(q+\delta q)\phi_0, \\ \Delta v + k_0^2(1+q)v &= -k_0^2\delta q\psi_1 - k_0^2\delta q\phi_0. \end{aligned}$$

In addition,  $\psi_1, \psi_2$ , and  $v$  satisfy the boundary condition (2.1.5).

Denote  $U = \psi_2 - \psi_1 - v$ . Then

$$\Delta U + k_0^2(1+q)U = -k_0^2\delta q(\psi_2 - \psi_1).$$

Similar arguments as in the proof of Lemma 2.2.3 give

$$\|U\|_{H^1(D)} \leq C \|\delta q\|_{L^\infty(D)} \|\psi_2 - \psi_1\|_{H^1(D)}.$$

From Lemma 2.2.3, we obtain further that

$$\|U\|_{H^1(D)} \leq C \|\delta q\|_{L^\infty(D)}^2 \|\phi_0\|_{L^2(D)}.$$

□

Finally, by combining the above lemmas, we arrive at

**Theorem 2.2.1.** *The scattering map  $M(q)$  is Fréchet differentiable with respect to  $q$  and its Fréchet derivative is*

$$DM(q) = \gamma T(q). \tag{2.2.15}$$

## 2.3 Inverse Medium Scattering

In this section, a regularized recursive linearization method for solving the inverse medium scattering problem of the Helmholtz equation in two dimensions is proposed. The algorithm, obtained by a continuation method on the spatial frequency of a one-parameter family of incident plane waves, requires only single-frequency scattering data. At each transverse part of the incident wave, the algorithm determines a forward model which produces the prescribed scattering data. Since the incident wave at a high spatial frequency can only penetrate a thin layer of the scatterer, the scattered field is weak. Consequently, the nonlinear equation becomes essentially linear, known as the Born approximation. The algorithm first solves this nearly linear equation at the largest  $|\eta|$  to obtain an approximation of the scatterer. This approximation is then used to linearize the nonlinear equation at the next smaller spatial frequency of the incident wave, which can penetrate a thicker layer of the scatterer, to produce a better approximation. When the spatial frequency,  $|\eta|$ , is smaller than the fixed wavenumber  $k_0$ , the incident wave becomes usual propagating plane wave, and the whole scatterer is illuminated. This process is continued until the spatial frequency is zero, where the

approximation of the scatterer is considered as the final reconstruction.

### 2.3.1 Born Approximation

Rewrite (2.1.4) as

$$\Delta\psi + k_0^2\psi = -k_0^2q(\phi_0 + \psi). \quad (2.3.1)$$

Consider a test function  $\psi_0 = e^{ik_0x \cdot \vec{d}}$ ,  $\vec{d} = (\cos\theta, \sin\theta)$ ,  $\theta \in [0, 2\pi]$ . Hence  $\psi_0$  satisfies (2.1.3).

Multiplying the equation (2.3.1) by  $\psi_0$ , and integrating over  $D$  on both sides, we have

$$\int_D \psi_0 \Delta\psi dx + k_0^2 \int_D \psi_0 \psi dx = -k_0^2 \int_D q(\phi_0 + \psi) \psi_0 dx.$$

Integration by parts yields

$$\int_D \psi \Delta\psi_0 dx + \int_{\partial D} \left( \psi_0 \frac{\partial\psi}{\partial n} - \psi \frac{\partial\psi_0}{\partial n} \right) ds + k_0^2 \int_D \psi_0 \psi dx = -k_0^2 \int_D q(\phi_0 + \psi) \psi_0 dx.$$

We have by noting (2.1.3) and the boundary condition (2.1.5) that

$$\int_D q(\phi_0 + \psi) \psi_0 dx = \frac{1}{k_0^2} \int_{\partial D} \psi \left( \frac{\partial\psi_0}{\partial n} - ik_0\psi_0 \right) ds.$$

Using the special form of the incident wave and the test function, we then get

$$\begin{aligned} \int_D q(x) e^{i(\eta + k_0 \cos\theta)x_1} e^{i(k(\eta) + k_0 \sin\theta)x_2} dx &= \frac{i}{k_0} \int_{\partial D} \psi(n \cdot \vec{d} - 1) e^{ik_0x \cdot \vec{d}} ds \\ &\quad - \int_D q\psi\psi_0 dx. \end{aligned} \quad (2.3.2)$$

From Lemma 2.2.3 and Remark 2.2.2, using an evanescent incident plane wave at a high spatial frequency, the scattered field is weak and the inverse scattering problem

becomes essentially linear. Dropping the nonlinear (second) term of (2.3.2), we obtain the linearized integral equation

$$\int_D q(x) e^{i(\eta + k_0 \cos \theta)x_1} e^{(-\sqrt{\eta^2 - k_0^2} + ik_0 \sin \theta)x_2} dx = \frac{i}{k_0} \int_{\partial D} \psi(n \cdot \vec{d} - 1) e^{ik_0 x \cdot \vec{d}} ds, \quad (2.3.3)$$

which is the Born approximation.

Since the scatterer  $q(x)$  has a compact support, (2.3.3) can be rewritten as

$$\int_0^{L_2} \hat{q}(\xi, x_2) e^{(-\sqrt{\eta^2 - k_0^2} + ik_0 \sin \theta)x_2} dx_2 = \frac{i}{k_0} \int_{\partial D} \psi(n \cdot \vec{d} - 1) e^{ikx \cdot \vec{d}} ds,$$

where  $\xi = \eta + k_0 \cos \theta$  and  $\hat{q}(\xi, x_2)$  is the Fourier transform of  $q(x)$  with respect to  $x_1$ . When the spatial frequency  $|\eta|$  is large, the incident wave penetrates a thin layer of the scatterer. Thus, the Born approximation allows a reconstruction containing information of the true scatterer in that thin layer. In [8, 4], the inversion involves data related to the scatterer through the Fourier transform in the case of weak scattering. Here, due to the presence of the evanescent wave, the inversion involves data related to the scatterer through a Fourier (with respect to  $x_1$ )-Laplace (with respect to  $x_2$ ) transform in the case of the weak scattering. Since the inversion of the Laplace transform is ill-posed, we consider the Landweber iteration to implement the linear integral equation (2.3.3) in order to reduce the computation cost and instability [29].

Define the data

$$f(\eta, \theta) = \begin{cases} \frac{i}{k_0} \int_{\partial D} \psi(n \cdot \vec{d} - 1) e^{ikx \cdot \vec{d}} ds & \text{for } |\eta| \geq \eta_{\max}, \\ 0 & \text{for } |\eta| < \eta_{\max}, \end{cases}$$

where  $\eta_{\max}$  is some large positive number.

The integral equation (2.3.3) can be written as the operator form

$$A(\eta, \theta; x)q(x) = f(\eta, \theta). \quad (2.3.4)$$

Following the idea of the Kaczmarz method, we use partial measurement data instead of using all them simultaneously for each sweep. Let  $\eta_i, i = 1, \dots, I$ , be the discretization of  $\eta$ , where  $I$  is the number of sweeps. Then we can rewrite (2.3.4) as

$$A(\eta_i, \theta; x)q(x) = f(\eta_i, \theta), \quad i = 1, \dots, I,$$

or in short

$$A_i q = f_i, \quad i = 1, \dots, I.$$

For each sweep  $i$ , the Landweber iteration takes the form

$$q_i^{(l)} = q_i^{(l-1)} + \alpha A_i^*(f_i - A(q_i^{(l-1)})), \quad l \in \mathbb{N},$$

where  $\alpha$  is a relaxation parameter. Since we just need an initial guess for the iteration in the recursive linearization, we only take one step Landweber iteration for each sweep, which yields

$$q_i = q_{i-1} + \alpha A_i^*(f_i - A(q_{i-1})), \quad i = 1, \dots, I, \quad (2.3.5)$$

where  $q_I$  is used as the starting point of the following recursive linearization algorithm.

## 2.3.2 Recursive Linearization

As discussed in the previous section, when the spatial frequency  $|\eta|$  is large, the Born approximation allows a reconstruction of the thin layer for the true scatterer. In this

section, a regularized recursive linearization method for solving the two-dimensional Helmholtz equation at fixed frequency is proposed.

Choose a large positive number  $\eta_{\max}$  and divide the interval  $[0, \eta_{\max}]$  into  $N$  subdivisions with the endpoints  $\{\eta_0, \eta_1, \dots, \eta_N\}$ , where  $\eta_0 = 0, \eta_N = \eta_{\max}$ , and  $\eta_{i-1} < \eta_i$  for  $1 \leq i \leq N$ . We intend to obtain  $q_\eta$  recursively at  $\eta = \eta_N, \eta_{N-1}, \dots, \eta_0$ .

Suppose now that the scatterer  $q_{\bar{\eta}}$  has been recovered at some  $\bar{\eta} = \eta_{i+1}$  and that  $\eta = \eta_i$  is slightly less than  $\bar{\eta}$ . We wish to determine  $q_\eta$ , or equivalently, to determine the perturbation

$$\delta q = q_\eta - q_{\bar{\eta}}.$$

For the reconstructed scatterer  $q_{\bar{\eta}}$ , we solve at the spatial frequency  $\eta$  the forward scattering problem

$$\Delta \tilde{\psi}^{(j, i)} + k_0^2(1 + q_{\bar{\eta}})\tilde{\psi}^{(j, i)} = -k_0^2 q_{\bar{\eta}} \phi_0^{(j, i)}, \quad (2.3.6)$$

$$\frac{\partial \tilde{\psi}^{(j, i)}}{\partial n} - ik_0 \tilde{\psi}^{(j, i)} = 0, \quad (2.3.7)$$

where the incident wave  $\phi_0^{(j, i)} = e^{i\eta_j x_1 + ik(\eta_j)x_2}$ ,  $|j| \geq i$ .

For the scatterer  $q_\eta$ , we have

$$\Delta \psi^{(j, i)} + k_0^2(1 + q_\eta)\psi^{(j, i)} = -k_0^2 q_\eta \phi_0^{(j, i)}, \quad (2.3.8)$$

$$\frac{\partial \psi^{(j, i)}}{\partial n} - ik_0 \psi^{(j, i)} = 0. \quad (2.3.9)$$

Subtracting (2.3.6), (2.3.7) from (2.3.8), (2.3.9) and omitting the second-order smallness in  $\delta q$  and in  $\delta\psi^{(j)} = \psi^{(j, i)} - \tilde{\psi}^{(j, i)}$ , we obtain

$$\Delta \delta\psi^{(j)} + k_0^2(1 + q_{\bar{\eta}})\delta\psi^{(j)} = -k_0^2 \delta q (\phi_0^{(j, i)} + \tilde{\psi}^{(j, i)}), \quad (2.3.10)$$

$$\frac{\partial \delta\psi^{(j)}}{\partial n} - ik_0 \delta\psi^{(j)} = 0. \quad (2.3.11)$$

For the scatterer  $q_\eta$  and the incident wave  $\phi_0^{(j,i)}$ , we define the map  $S_j(q_\eta, \phi_0^{(j,i)})$  by

$$S_j(q_\eta, \phi_0^{(j,i)}) = \psi^{(j,i)},$$

where  $\psi^{(j,i)}$  is the scattering data corresponding to the incident wave  $\phi_0^{(j,i)}$ . Let  $\gamma$  be the trace operator to the boundary  $\partial D$ . Define the scattering map

$$M_j(q_\eta, \phi_0^{(j,i)}) = \gamma S_j(q_\eta, \phi_0^{(j,i)}).$$

For simplicity, denote  $M_j(q_\eta, \phi_0^{(j,i)})$  by  $M_j(q_\eta)$ . By the definition of the trace operator, we have

$$M_j(q_\eta) = \psi^{(j,i)}|_{\partial D}.$$

Let  $DM_j(q_{\tilde{\eta}})$  be the Fréchet derivative of  $M_j(q_\eta)$  and denote the residual operator by

$$R_j(q_{\tilde{\eta}}) = \psi^{(j,i)}|_{\partial D} - \tilde{\psi}^{(j,i)}|_{\partial D}.$$

It follows from Theorem 2.2.1 that

$$DM_j(q_{\tilde{\eta}})\delta q = R_j(q_{\tilde{\eta}}). \quad (2.3.12)$$

Similarly, in order to reduce the computation cost and instability, we consider the Landweber iteration of (2.3.12), which has the form

$$\delta q = \beta DM_j^*(q_{\tilde{\eta}})R_j(q_{\tilde{\eta}}), \quad \text{for all } |j| \geq i, \quad (2.3.13)$$

where  $\beta$  is a relaxation parameter and  $DM_j^*(q_{\tilde{\eta}})$  is the adjoint operator of  $DM_j(q_{\tilde{\eta}})$ .

In order to compute the correction  $\delta q$ , we need some efficient way to compute  $DM_j^*(q_{\tilde{\eta}})R_j(q_{\tilde{\eta}})$ , which is given by the following theorem.

**Theorem 2.3.1.** *Given residual  $R_j(q_{\bar{\eta}})$ , there exists a function  $\phi^{(j,i)}$  such that the adjoint Fréchet derivative  $DM_j^*(q_{\bar{\eta}})$  satisfies*

$$[DM_j^*(q_{\bar{\eta}})R_j(q_{\bar{\eta}})](x) = k_0^2(\overline{\phi_0^{(j,i)}}(x) + \overline{\tilde{\psi}^{(j,i)}}(x))\phi^{(j,i)}(x), \quad (2.3.14)$$

where  $\phi_0^{(j,i)}$  is the incident wave and  $\tilde{\psi}^{(j,i)}$  is the solution of (2.3.6), (2.3.7) with the incident wave  $\phi_0^{(j,i)}$ .

**PROOF.** Let  $\tilde{\psi}^{(j,i)}$  be the solution of (2.3.6), (2.3.7) with the incident wave  $\phi_0^{(j,i)}$ .

Consider the following problem

$$\Delta\delta\psi^{(j)} + k_0^2(1 + q_{\bar{\eta}})\delta\psi^{(j)} = -k_0^2\delta q(\phi_0^{(j,i)} + \tilde{\psi}^{(j,i)}), \quad (2.3.15)$$

$$\frac{\partial\delta\psi^{(j)}}{\partial n} - ik_0\delta\psi^{(j)} = 0. \quad (2.3.16)$$

and the adjoint problem

$$\Delta\phi^{(j,i)} + k_0^2(1 + q_{\bar{\eta}})\phi^{(j,i)} = 0, \quad (2.3.17)$$

$$\frac{\partial\phi^{(j,i)}}{\partial n} + ik_0\phi^{(j,i)} = R_j(q_{\bar{\eta}}). \quad (2.3.18)$$

Since the existence and uniqueness of the weak solution for the adjoint problem may be established by following the same proof of Lemma 2.2.2, we omit the proof here.

Multiplying the equation (2.3.15) with the complex conjugate of  $\phi^{(j,i)}$  and integrating over  $D$  on both sides, we obtain

$$\int_D \overline{\phi^{(j,i)}} \Delta\delta\psi^{(j)} dx + k_0^2 \int_D (1 + q_{\bar{\eta}}) \delta\psi^{(j)} \overline{\phi^{(j,i)}} dx = -k_0^2 \int_D \delta q (\phi_0^{(j,i)} + \tilde{\psi}^{(j,i)}) \overline{\phi^{(j,i)}} dx.$$

Integration by parts yields

$$\int_{\partial D} \left( \overline{\phi^{(j,i)}} \frac{\partial \delta \psi^{(j)}}{\partial n} - \delta \psi^{(j)} \frac{\partial \overline{\phi^{(j,i)}}}{\partial n} \right) ds = -k_0^2 \int_D \delta q (\phi_0^{(j,i)} + \tilde{\psi}^{(j,i)}) \overline{\phi^{(j,i)}} dx.$$

Using the boundary condition (2.3.16), we deduce

$$\int_{\partial D} \delta \psi^{(j)} \left( \frac{\partial \overline{\phi^{(j,i)}}}{\partial n} - ik_0 \overline{\phi^{(j,i)}} \right) ds = k_0^2 \int_D \delta q (\phi_0^{(j,i)} + \tilde{\psi}^{(j,i)}) \overline{\phi^{(j,i)}} dx.$$

It follows from (2.3.12) and the boundary condition (2.3.18) that

$$\int_{\partial D} [DM_j(q_{\tilde{\eta}}) \delta q] \overline{R_j(q_{\tilde{\eta}})} ds = k_0^2 \int_D \delta q (\phi_0^{(j,i)} + \tilde{\psi}^{(j,i)}) \overline{\phi^{(j,i)}} dx.$$

We know from the adjoint operator  $DM_j^*(q_{\tilde{\eta}})$  that

$$\int_D \delta q \overline{DM_j^*(q_{\tilde{\eta}}) R_j(q_{\tilde{\eta}})} dx = k_0^2 \int_D \delta q (\phi_0^{(j,i)} + \tilde{\psi}^{(j,i)}) \overline{\phi^{(j,i)}} dx.$$

Since it holds for any  $\delta q$ , we have

$$\overline{DM_j^*(q_{\tilde{\eta}}) R_j(q_{\tilde{\eta}})} = k_0^2 (\phi_0^{(j,i)} + \tilde{\psi}^{(j,i)}) \overline{\phi^{(j,i)}}.$$

Taking the complex conjugate of the above equation yields the result.  $\square$

Using this theorem, we can rewrite (2.3.13) as

$$\delta q = k_0^2 \beta (\overline{\phi_0^{(j,i)} + \tilde{\psi}^{(j,i)}}) \phi^{(j,i)}. \quad (2.3.19)$$

So for each incident wave with a transverse part  $\eta_j$ , we have to solve one forward problem (2.3.6), (2.3.7) along with one adjoint problem (2.3.17), (2.3.18). Since the adjoint problem has a similar variational form as the forward problem. Essentially, we need to compute two forward problems at each sweep. Once  $\delta q$  is determined,  $q_{\tilde{\eta}}$  is

---

```

Initialization
   $\eta_N = \eta_{\max}$    largest  $\eta_{\max}$ 
   $q_{\eta_{\max}}$    Born approximation
Reconstruction loop:
  FOR  $i = N : 0$  ( $\eta_i = \eta_{\max} : \eta_0$ )   march along spatial frequency
    FOR  $j = N : i$  ( $|\eta_j| = \eta_{\max} : \eta_i$ )   perform refinement
      solve (2.3.6), (2.3.7) for  $\tilde{\psi}^{(j, i)}$    one forward problem
      solve (2.3.17), (2.3.18) for  $\phi^{(j, i)}$    one adjoint problem
       $\delta q_i^j = k_0^2 \beta(\phi_0^{(j, i)} + \tilde{\psi}^{(j, i)}) \phi^{(j, i)}$ 
       $q_i^j := q_i^j + \delta q_i^j$ 
    END
     $q_i := q_i^i$ 
  END
   $q := q_0$    final reconstruction

```

---

Table 2.1. Recursive linearization reconstruction algorithm.

updated by  $q_{\tilde{\eta}} + \delta q$ . After completing sweeps with  $|\eta_j| \geq \eta$ , we get the reconstructed scatterer  $q_\eta$  at the spatial frequency  $\eta$ .

**Remark 2.3.1.** *For given  $\eta_i$ , iterations for  $|\eta_j| \geq \eta_i$  could be repeated to improve the accuracy of the approximation for  $q_{\eta_i}$ . However, in practice, this refinement is usually unnecessary because of the slow convergence of the Landweber iteration at the same stage [14], i.e. without using essentially different data. Numerical results show that the iterative process described as the reconstruction loop in Table 2.1 is sufficient to obtain reasonable accuracy.*

The recursive linearization for inverse medium scattering at fixed frequency is summarized in Table 2.1.

## 2.4 Numerical Experiments

In this section, we discuss the numerical solution of the forward scattering problem and the computational issues of the recursive linearization algorithm.

The scattering data are obtained by numerical solution of the forward scattering problem. As for the forward solver, we adopt the finite element method (FEM), which leads to a sparse matrix. The sparse large-scale linear system can be most efficiently solved if the zero elements of coefficient matrix are not stored. We used the commonly used compressed row storage (CRS) format which makes no assumptions about the sparsity structure of the matrix and does not store any unnecessary elements. In fact, from the variational formula of our direct problem (2.2.1), the coefficient matrix is complex symmetric. Hence, only the lower triangular portion of the matrix needs be stored. Regarding the linear solver, either biconjugate gradient (BiCG) or quasi-minimal residual (QMR) algorithms with diagonal preconditioning may be used to solve the sparse, symmetric, and complex system of the equations. For our examples, it appears that the QMR is more efficient.

In the following, to illustrate the performance of the algorithm, three numerical examples are presented for reconstructing the scatterer of the Helmholtz equation in two dimensions. For stability analysis, some relative random noise is added to the data, i.e. the electric field takes the form

$$\psi|_{\partial D} := (1 + \sigma \text{rand})\psi|_{\partial D}.$$

Here,  $\text{rand}$  gives uniformly distributed random numbers in  $[-1, 1]$  and  $\sigma$  is a noise level parameter taken to be 0.02 in our numerical experiments. The relaxation parameter

$\beta$  is taken to be 0.01. Define the relative error by

$$e_2 = \frac{(\sum_{i,j} |q_{ij} - \bar{q}_{ij}|^2)^{1/2}}{(\sum_{i,j} |q_{ij}|^2)^{1/2}},$$

where  $\bar{q}$  is the reconstructed scatter and  $q$  is the true scatterer.

Example 1. Let

$$q(x_1, x_2) = 0.3(1 - x_1)^2 e^{-x_1^2 - (x_2 + 1)^2} - \left(\frac{x_1}{5} - x_1^3 - x_2^5\right) e^{-(x_1^2 + x_2^2)} - \frac{1}{30} e^{-(x_1 + 1)^2 - x_2^2},$$

reconstruct a scatterer defined by

$$q_1(x_1, x_2) = q(3x_1, 3(x_2 - 1)) \quad (2.4.1)$$

inside the domain  $D = [-1, 1] \times [0, 2]$ . See Figure 2.3 for the surface plot of the scatterer function. Figure 2.10 is the final reconstruction using the wavenumber  $k_0 = 10.0$  and the step size of the spatial frequency  $\delta\eta = 0.6$ . Figures 2.4-2.9 show the evolution of reconstructions at different spatial frequencies. Figure 2.11 presents the effect of the wavenumber  $k_0$  on the result of reconstruction, which illustrates clearly that the inversion using a larger wavenumber  $k_0$  is better than that using a smaller one. This result may be explained by Heisenberg's uncertainty principle [8, 9]. Figure 2.12 shows the relative error by using different step size of the spatial frequency, which suggests that we may use a large step size in order to save computation cost since the final reconstruction is not really sensitive to the step size.

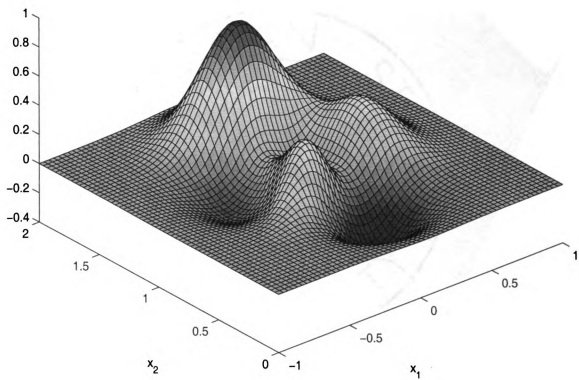


Figure 2.3. Example 1: true scatterer  $q_1$ .

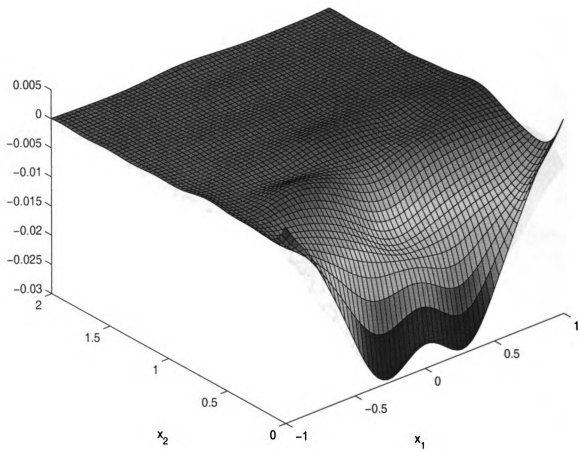


Figure 2.4. Example 1: Born approximation.

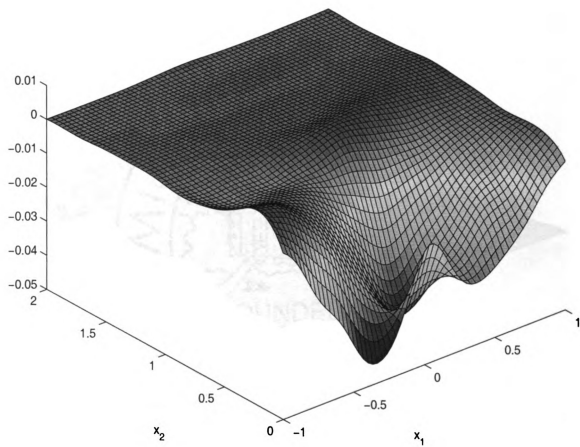


Figure 2.5. Example 1: reconstruction of  $q_1$  at  $\eta = 10.2$ .

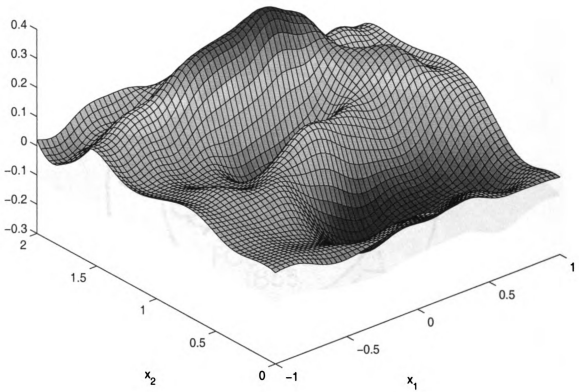


Figure 2.6. Example 1: reconstruction of  $q_1$  at  $\eta = 8.4$ .

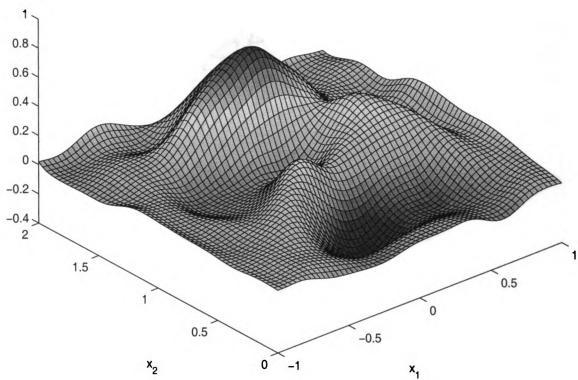


Figure 2.7. Example 1: reconstruction of  $q_1$  at  $\eta = 6.6$ .

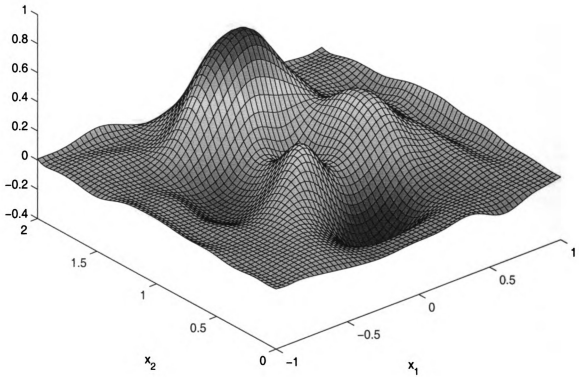


Figure 2.8. Example 1: reconstruction of  $q_1$  at  $\eta = 4.8$ .

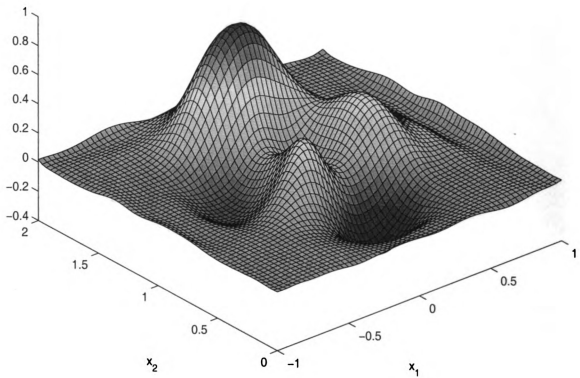


Figure 2.9. Example 1: reconstruction of  $q_1$  at  $\eta = 3.0$ .

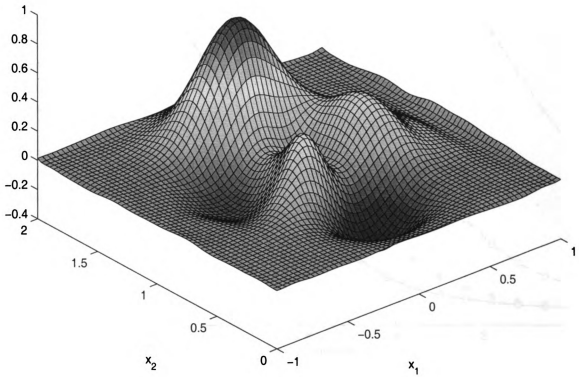


Figure 2.10. Example 1: reconstruction of  $q_1$  at  $\eta = 0.0$ .

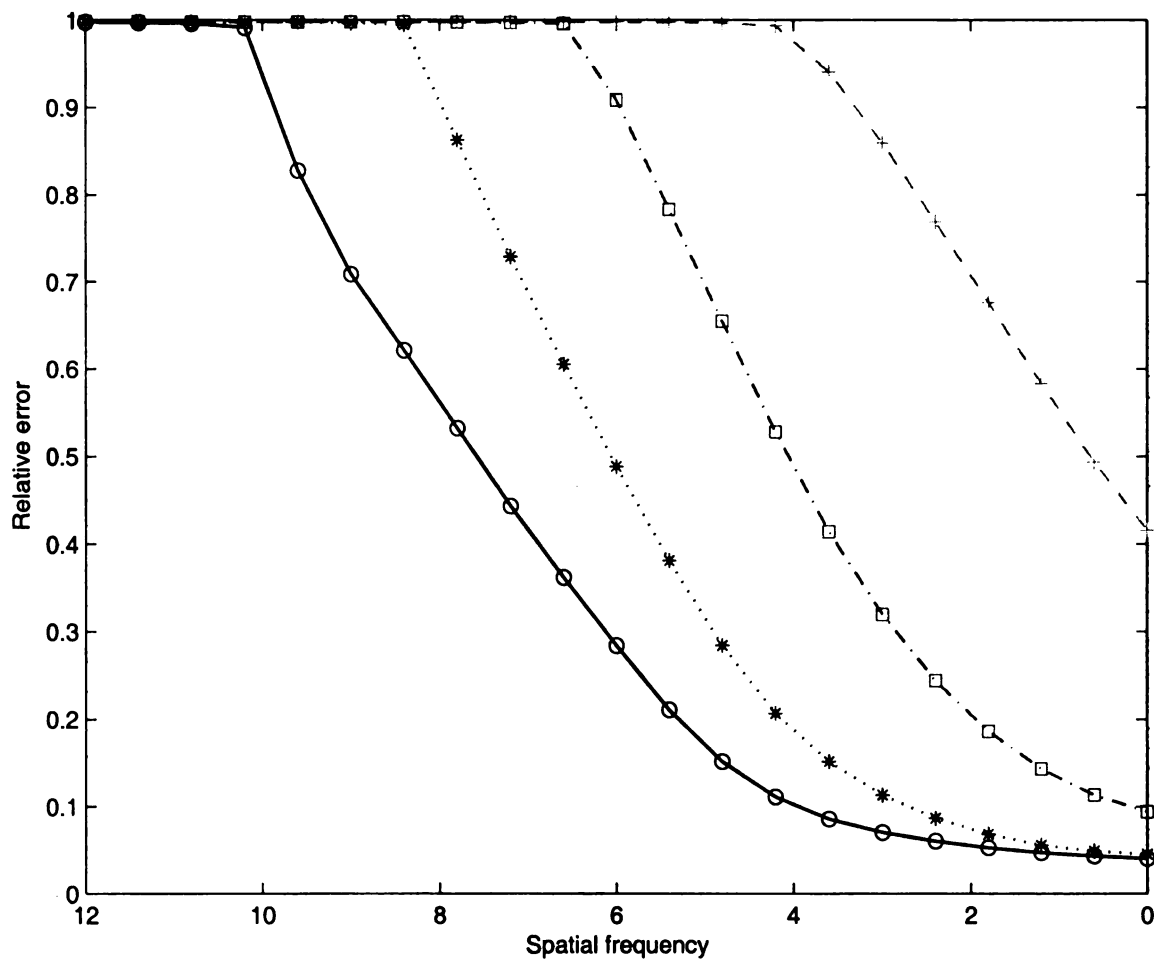


Figure 2.11. Example 1. Relative error of the reconstruction  $q_1$  at different wavenumber  $k_0$ .  $\circ$ : reconstruction at  $k_0 = 10.0$ ;  $*$ : reconstruction at  $k_0 = 8.0$ ;  $\square$ : reconstruction at  $k_0 = 6.0$ ;  $+$ : reconstruction at  $k_0 = 4.0$ .

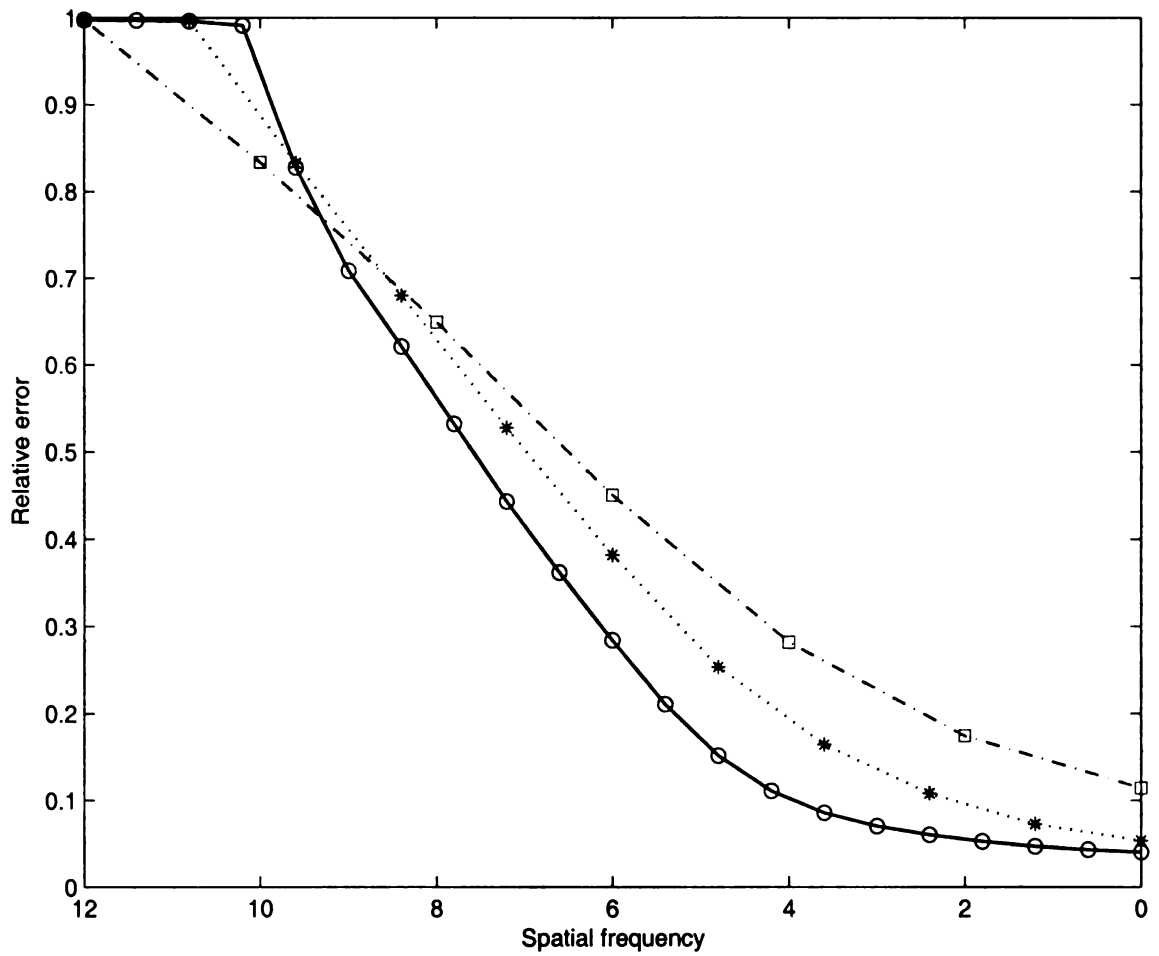


Figure 2.12. Example 1. Relative error of the reconstruction  $q_1$  at different step size  $\delta\eta$ .  $\circ$ : reconstruction at  $\delta\eta = 0.6$ ;  $*$ : reconstruction at  $\delta\eta = 1.2$ ;  $\square$ : reconstruction at  $\delta\eta = 2.0$ .

Example 2. Reconstruct a scatterer defined in  $D$  by

$$q_2(x_1, x_2) = \begin{cases} q_1(x_1/0.8, x_2/0.8) & \text{for } x_1^2 + (x_2 - 1)^2 \leq 0.747^2, \\ -0.3, & \text{for } 0.747^2 < x_1^2 + (x_2 - 1)^2 \leq 0.853^2, \\ 0, & \text{for } x_1^2 + (x_2 - 1)^2 > 0.853^2. \end{cases}$$

See Figures 2.13 and (2.15) for the surface and contour plots of the function. It is easily seen that this scatterer is difficult to reconstruct because of the discontinuity across two circles. The example could be regarded as a model problem for ultrasound tomography of a human head, where the skull is represented by the thin layer of denser material in the narrow annulus region. Figures 2.14 and 2.16 show the surface and contour plots of the reconstructed scatterer using the wavenumber  $k_0 = 15.0$  and the step size  $\delta\eta = 0.85$ . Figure 2.17 gives the evolution of reconstruction horizontally across the diameter. An examination of the plots shows that the error of the reconstructions occurs largely around the discontinuities, while the smooth part is recovered more accurately. As expected, the Gibbs phenomenon appears in the reconstructed scatterer near the discontinuity.

Example 3. Reconstruct a scatterer defined in  $D$  by

$$q_3(x_1, x_2) = \begin{cases} \cos(2.5\pi r_1) & \text{for } r_1 \leq 0.2, \\ \cos(2.5\pi r_2) & \text{for } r_2 \leq 0.2, \\ 0 & \text{otherwise,} \end{cases}$$

where  $r_1 = \sqrt{(x_1 + 0.25)^2 + (x_2 - 1.0)^2}$  and  $r_2 = \sqrt{(x_1 - 0.25)^2 + (x_2 - 1.0)^2}$ . The compact support of this scatterer is two isolated disks with the same radius of 0.2 and the centers at  $(-0.25, 1.0)$  and  $(0.25, 1.0)$ . See Figures 2.18 and 2.20 for the surface plot and image of the function. Figures 2.19 and 2.21 are the final reconstruction using the wavenumber  $k_0 = 3\pi$  and the step size of the spatial frequency  $\delta\eta = 0.6$ .

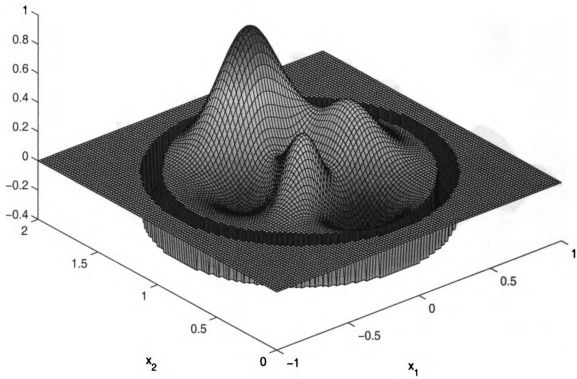


Figure 2.13. Example 2: true scatterer of  $q_2$ .

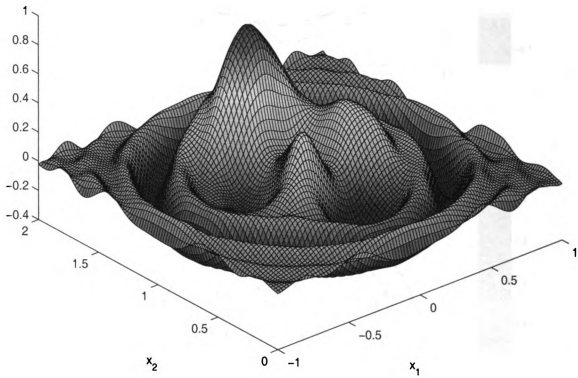


Figure 2.14. Example 2: reconstruction of  $q_2$ .

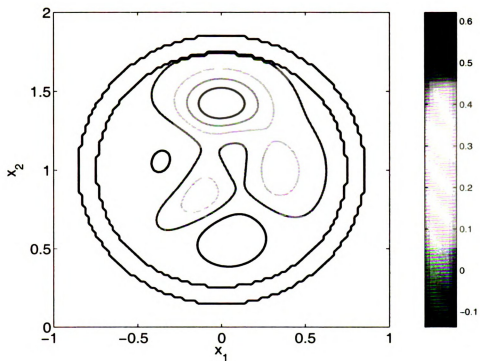


Figure 2.15. Example 2: contour view of the true scatterer  $q_2$ .

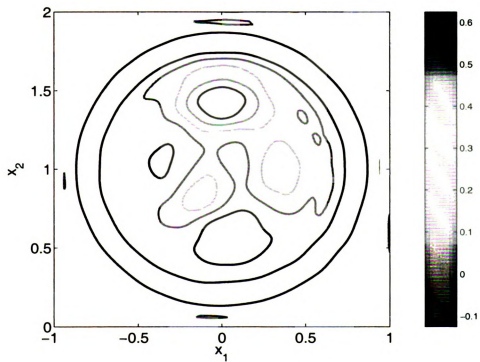


Figure 2.16. Example 2: contour view of the reconstructed scatterer  $q_2$ .

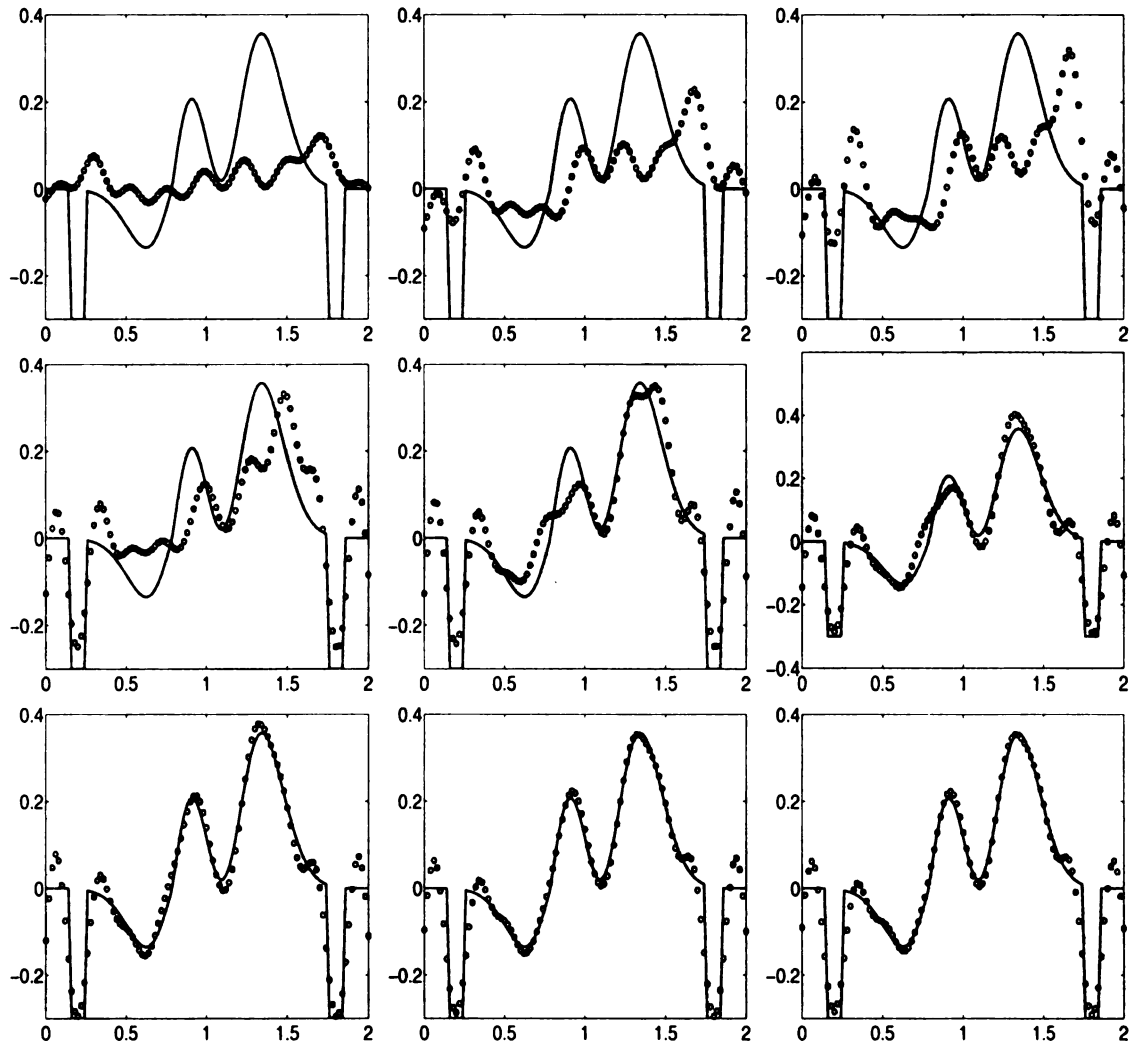


Figure 2.17. Example 2. Evolution of slice for the reconstruction  $q_2$ . Solid line: true scatterer; Circle: reconstruction. Top row from left to right: reconstruction at  $\eta = 14.45$ ; reconstruction at  $\eta = 13.60$ ; reconstruction at  $\eta = 12.75$ ; middle row from left to right: reconstruction at  $\eta = 10.20$ ; reconstruction at  $\eta = 8.50$ ; reconstruction at  $\eta = 6.80$ ; bottom row from left to right: reconstruction at  $\eta = 5.10$ ; reconstruction at  $\eta = 2.55$ ; reconstruction at  $\eta = 0.0$ .

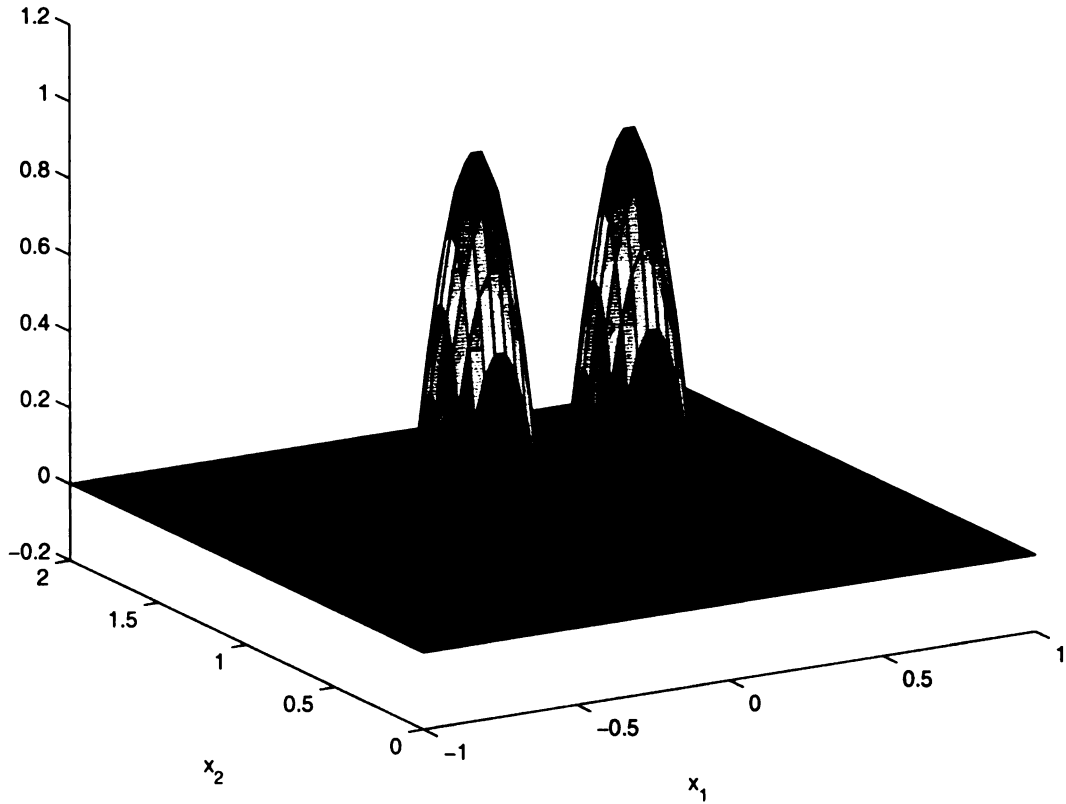


Figure 2.18. Example 3: true scatterer of  $q_3$ .

This example is used to examine the resolution of the reconstructed image. In this numerical experiment, the wavelength of the incident plane waves is  $2\pi/k_0 = 0.6$ . The distance of the centers for the compact support is 0.5, which is less than one wavelength. From the well separated bumps, the resolution of the image is clearly in the scale of subwavelength. The subwavelength resolution is expected since evanescent waves are used for illumination.

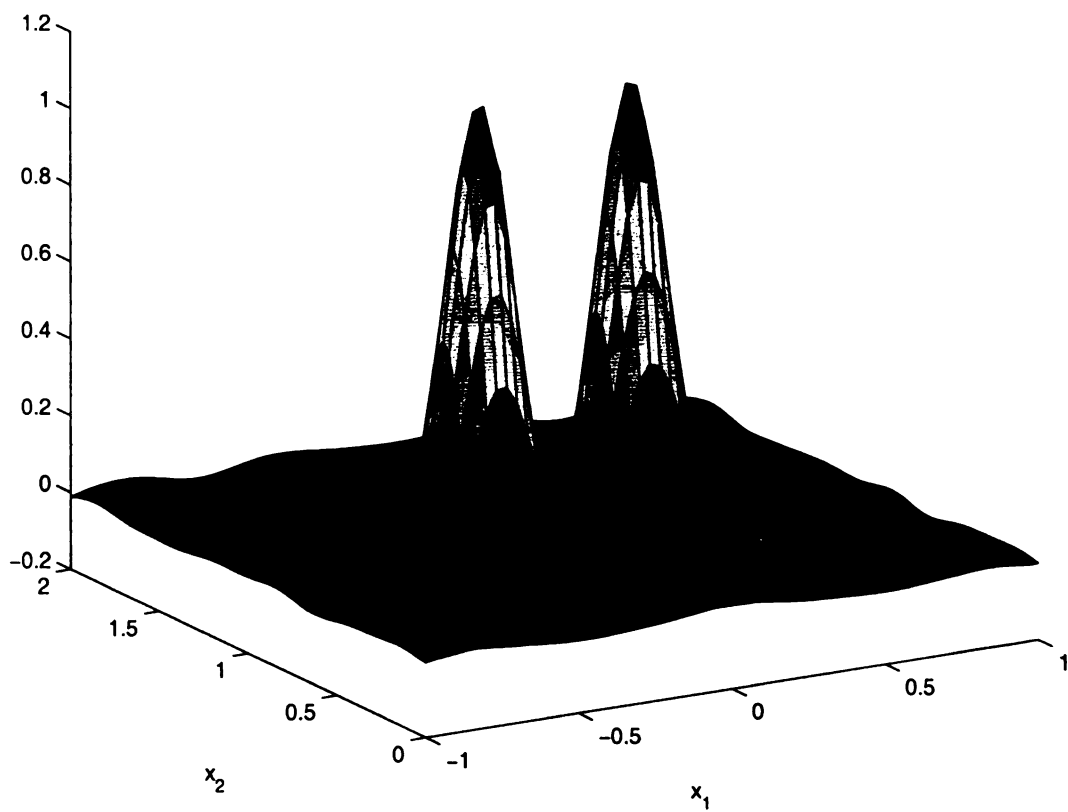


Figure 2.19. Example 3: reconstructed scatterer of  $q_3$ .

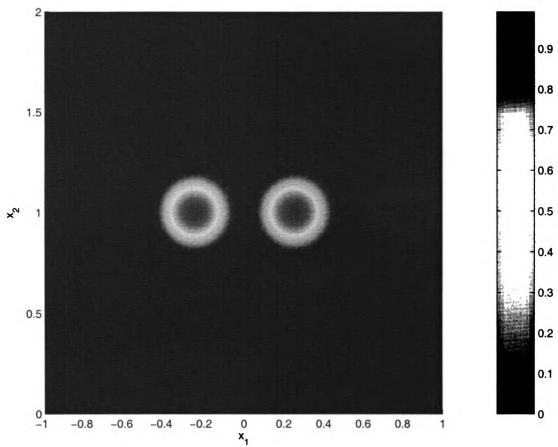


Figure 2.20. Example 3: image view of the true scatterer  $q_3$ .

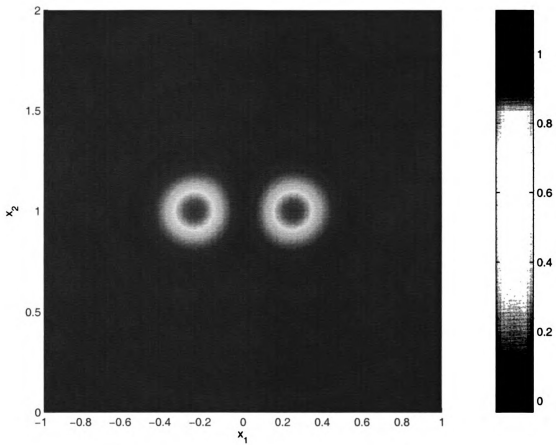


Figure 2.21. Example 3: image view of the reconstructed scatterer  $q_3$ .

## 2.5 Concluding Remarks

We have presented a new continuation method with respect to the spatial frequency of a one-parameter family of plane waves. The recursive linearization algorithm is robust and efficient for solving the inverse medium scattering at fixed frequency. Finally, we point out some future directions along the line of this work. The first is concerned with the convergence analysis. Although our numerical experiments demonstrate the convergence and stability of the inversion algorithm, no rigorous mathematical result is available at present. Another direction is to investigate inverse medium problems for Maxwell's equations at fixed frequency. We are currently attempting to extend the approach in this paper to the more complicated 3D model problems and will report the progress elsewhere.

## BIBLIOGRAPHY

- [1] H. Ammari and G. Bao, *Analysis of the scattering map of a linearized inverse medium problem for electromagnetic waves*, Inverse Problems, 17(2001), 219-234.
- [2] G. Bao, Y. Chen, and F. Ma, *Regularity and stability for the scattering map of a linearized inverse medium problem*, J. Math. Anal. Appl., 247(2000), 255-271.
- [3] G. Bao and J. Liu, *Numerical solution of inverse scattering problems with multi-experimental limited aperture data*, SIAM J. Sci. Comput., 25(2003), 1102-1117.
- [4] G. Bao and P. Li, *Inverse medium scattering problems for electromagnetic waves*, SIAM J. Appl. Math., to appear.
- [5] G. Bao and P. Li, *Inverse medium scattering for Helmholtz equation at fixed frequency*, Inverse Problems, submitted.
- [6] P. Carney and J. Schotland, *Three-dimensional total internal reflection microscopy*, Opt. Lett., 26(2001), 1072-1074.
- [7] P. Carney and J. Schotland, *Near-field tomography*, MSRI Series in Mathematics and Its Applications, 47(2003), 131-166.
- [8] Y. Chen, *Inverse scattering via Heisenberg uncertainty principle*, Inverse Problems, 13(1997), 253-282.
- [9] Y. Chen, *Inverse scattering via skin effect*, Inverse Problems, 13(1997), 649-667.
- [10] D. Colton and R. Kress, *Inverse Acoustic and Electromagnetic Scattering Theory*, 2nd ed., Appl. Math. Sci. 93, Springer-Verlag, Berlin, 1998.
- [11] D. Courjon, *Near-field Microscopy and Near-field Optics*, Imperial College Press, 2003.
- [12] D. Courjon and C. Bainier, *Near field microscopy and near field optics*, Rep. Prog. Phys., 57(1994), 989-1028.

- [13] O. Dorn, H. Bertete-Aguirre, J. G. Berryman, and G. C. Papanicolaou, *A nonlinear inversion method for 3D electromagnetic imaging using adjoint fields*, *Inverse Problems*, 15(1999), 1523-1558.
- [14] H. Engl, M. Hanke, and A. Neubauer, *Regularization of Inverse Problems*, Dordrecht: Kluwer, 1996.
- [15] M. Eller, V. Isakov, G. Nakamura, and D. Tataru, *Uniqueness and stability in the Cauchy problem for Maxwell's and elasticity system*, *Nonlinear Partial Differential Equation 14*, College de France Seminar, Eds. D. Cioranescu, J. L. Lions, *Studies in Mathematics and its Applications*, 31(2002), 329-350.
- [16] N.E. Gibbs, W.G. Poole, Jr., and P.K. Stockmeyer, *An algorithm for reducing bandwidth and profile of a sparse matrix*, *SIAM J. Numer. Anal.*, 13(1976), 236-250.
- [17] D. Gilbarg and N. Trudinger, *Elliptic Partial Differential Equations of Second Order*, Springer-Verlag, New York, 1983.
- [18] C. Girard and A. Dereux, *Near-field optics theories*, *Rep. Prog. Phys.*, 59(1996), 657-699.
- [19] T. Hohage, *On the numerical solution of a three-dimensional inverse medium scattering problem*, *Inverse Problems*, 17(2001), 1743-1763
- [20] H. Haddar and P. Monk, *The linear sampling method for solving the electromagnetic inverse medium problem*, *Inverse Problems*, 18(2002), 891-906.
- [21] D. Jerison and C. Kenig, *Unique continuation and absence of positive eigenvalues for Schrödinger operators*, *Ann. Math.*, 121(1985), 463-488.
- [22] J. Jin, *The Finite Element Methods in Electromagnetics*, John Wiley & Sons, 2002.
- [23] A. Kameari, *Symmetric second order edge elements for triangle and tetrahedra*, *IEEE Trans. Magn.*, 35(1999) 1394-1397.
- [24] R. G. Keys and A. B. Weglein, *Generalized linear inversion and the first Born theory for acoustic media*, *J. Math. Phys.*, 24(1983), 1444-1449.
- [25] A. Kirsch and P. Monk, *A finite element/spectral method for approximating the time-harmonic Maxwell's system in  $\mathbb{R}^3$* , *SIAM J. Appl. Math.*, 55(1995), 1324-1344.

- [26] A. Kirsch and P. Monk, *Corrigendum: A finite element/spectral method for approximating the time-harmonic Maxwell's system in  $\mathbb{R}^3$* , SIAM J. Appl. Math., 58(1998), 2024-2028.
- [27] A. Kirsch and P. Monk, *A finite element method for approximating electromagnetic scattering from a conducting object*, Numer. Math., 92(2002), 501-534.
- [28] P. Monk, *Finite Element Methods for Maxwell's Equations*, Oxford University Press, Oxford, 2003.
- [29] F. Natterer, *The Mathematics of Computerized Tomography*, Stuttgart: Teubner, 1986.
- [30] F. Natterer and F. Wübbeling, *A propagation-backpropagation method for ultrasound tomography*, Inverse Problems, 11(1995), 1225-1232.
- [31] J. C. Nédélec, *Mixed finite elements in  $\mathbb{R}^3$* , Numer. Math., 35(1980), 315-341.
- [32] J. C. Nédélec, *Acoustic and Electromagnetic Equations: Integral Representations for Harmonic Problems*, Springer, New York, 2000.
- [33] L. Rudin, S. Osher, and E. Fatemi, *Nonlinear total variation based noise removal algorithms*, Physica D, 60(1992), 259-268.
- [34] M. Vögeler, *Reconstruction of the three-dimensional refractive index in electromagnetic scattering by using a propagation-backpropagation method*, Inverse Problems, 19(2003), 739-753.

MICHIGAN STATE UNIVERSITY



3 1293 02736